Shock resistance of elastomer-strengthened metallic corrugated core sandwich panels

Xin Wang [a,b], Chao He [c,d], Zengshen Yue [a], Xue Li [c,d], Runpei Yu [a], Haibo Ji [c,d], Zhenyu Zhao [c,d], Qiancheng Zhang [a,*], Tian Jian Lu [c,d,**]

[a] State Key Laboratory for Strength and Vibration of Mechanical Structures, Xi'an Jiaotong University, Xi'an, 710049, China
[b] Impact Mechanics Laboratory, National University of Singapore, Singapore, 117575, Singapore
[c] State Key Laboratory of Mechanics and Control of Mechanical Structures, Nanjing University of Aeronautics and Astronautics, Nanjing, 210016, China
[d] MIIT Key Laboratory of Multifunctional Lightweight Materials and Structures, Nanjing University of Aeronautics and Astronautics, Nanjing, 210016, China

ARTICLE INFO

ABSTRACT

How polyurea coating affects the shock resistance of fully-clamped metallic corrugated core sandwich panels against high-velocity aluminum foam projectile impact is systematically elucidated via a mixed experimental and numerical investigation. Dynamic deformation process, deformation/failure modes, and permanent deflections of polyurea-coated sandwich panels are testified at various projectile momentum and compared with those of non-coated sandwich panels. A high-fidelity finite element (FE) model considering both rate-dependent compressive and tensile behaviors of polyurea elastomer is established and employed to simulate the dynamic response of polyurea-coated sandwich panels, interrogate the underlying enhancement mechanisms, and estimate the effects of projectile momentum and coating thickness/area/position upon permanent mid-span deflection and energy absorption. Reasonable agreement is realized between FE predictions and measurements. The presence of polyurea coating helps curtail permanent deflection in the central region and avoid shear failure around the clamping area. The benefit of polyurea coating on mitigating impact deformation remains stable as the projectile momentum is varied over a broad range, and the use of thicker, larger, and impact-side coating is preferred. The observed performance improvement is attributed mainly to enhanced plastic bending moment and membrane force in the polyurea-coated sandwich panel. The results of this study open up a new avenue to enhance the shock resistance of metallic sandwich structures subjected to impulsive loading.

1. Introduction

Ultralight all-metallic sandwiches encompassing thin face sheets and lattice truss cores outperform traditional monolithic/stiffened plates when subjected to intense blast loading, exhibiting outstanding survivability [1–9]. The benefits of such sandwich construction have been attributed to Refs. [10,11]: (i) lower momentum transferred to the sandwich by virtue of fluid-structure interaction; (ii) substantial plastic crushing and preeminent energy absorption of cellular core; (iii) enhanced plastic flexural strength due to sandwich construction. As core topology significantly affects the shock resistance of a sandwich structure, core designs that take into account simultaneous crushing and stretching resistance are preferred [12–19]. Among numerous

topologies, corrugated cores (also called fold plates or prismatic lattice cores) have been ranked as one of the most desirable sandwich cores for blast/impact-resistant applications, due to their high collapse resistance, high longitudinal stretching/shear strength, and relatively low fabrication expense.

Over the past two decades, the dynamic responses of corrugated core sandwich structures to a variety of shock loadings (e.g., air blast, underwater blast, soil blast, simulated blast, and the like) have been extensively studied [20–26]. For instance, direct experimental observation on quasi-static and dynamic crushing process of corrugated cores was presented [27], while the corresponding deformation mechanisms were attributed, depending upon the loading rate, to three dominant regimes: plastic buckling, buckle-wave, and stubbing [28]. In addition to
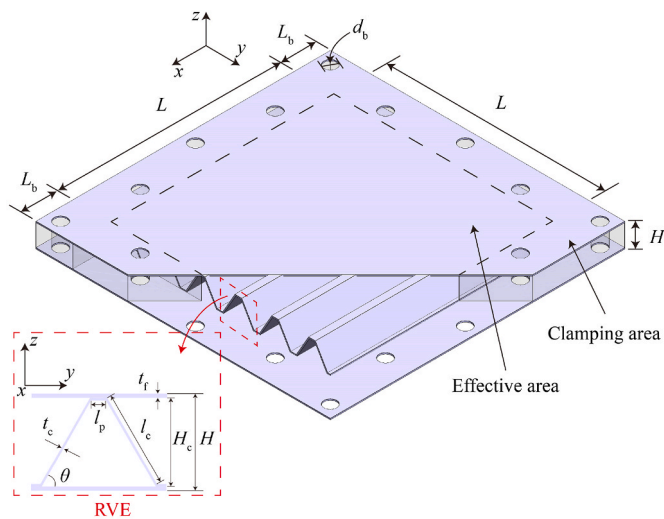

Fig. 1. Geometric schematic of a corrugated core sandwich panel to be fabricated.

studying the dynamic response of corrugated core sandwich beams/plates to localized foam projectile impact, the effects of impact momentum and core orientation on shock resistance were also ascertained [23,24]. Similarly, the mechanical behaviors of corrugated core sandwich construction under air/underwater blast loading were systematically elucidated [20,21,29]. Further, an optimization study performed with the method of finite elements (FE) demonstrated that sandwich panels with corrugated cores exhibited better blast resistance than those with square honeycomb and pyramidal lattice cores [30]. Nonetheless, a fundamental shortcoming of corrugated core sandwich structures was also identified [23,24]. That is, these structures need to be used as appropriate, for large structural deformation may lead to severe failure at a lower level of shock loading relative to monolithic plates. Therefore, to sustain structural integrity throughout an extensive range of shock loading, practical strategies to retrofit and strengthen corrugated core sandwich construction need to be developed.

Recently, the concept of hybrid sandwich cores has attracted intense research interest [31]. Owing to core topology, filling or in-situ synthesizing various materials into corrugated cores appears convenient. Thus, the strategy of constructing hybrid cores is presenting promising opportunities to enhance shock resistance of the existing structures. For instance, considerable attention has been paid to exploring novel hybrid core designs for blast/impact applications, including the corrugated core filled with metal foam [32], polymer foam [33], water [25], sand [26], gravel [34], ceramic [35], concrete [36], and so on. The existing observations have confirmed that the presence of hybrid cores curtails the permanent deformation of sandwich structures, but the benefit seems to diminish gradually with the increase of shock loading [25,26]. To the authors' knowledge, this is because the large deformation of sandwich structures is dominated by membrane stretching strength rather than plastic bending moment, and the contribution of sandwich cores to stretching resistance of the whole structures is less than that of metal face sheets. Thus, similar to the idea of hybrid cores, constructing "hybrid face sheets" encompassing stretch-resistant compliant materials and metal face sheets is also a fascinating option. To date, few studies have focused on this strategy to improve the blast and impact resistance

of metallic corrugated core sandwiches.

Retrofitting a metallic plate with elastomer coating has been widely considered as a rapid and effective strategy to improve its survivability, especially when subjected to intense blast/impact loading [37]. For typical instance, after the 9/11 terrorist attacks, the U.S. Air Force & Navy started to spray polyurea coating on building and marine construction to help maintain structural integrity during intense blast loading [38,39]. Subsequently, although in-depth experimental and numerical insights have been brought into the potential of polyurea for retrofitting applications, the underlying mechanisms behind its remarkable blast/impact mitigation effects are usually comprehended at different scales [40]. From the macro-scale, Xue and Hutchinson [41,42] ascertained a substantial increase of necking limit and energy absorption in metal-elastomer bilayers under both quasi-static and dynamic stretching. Amini et al. [43,44] further testified that the benefit of polyurea coating depends on its relative position on metal substrate due to the initial shock effect, the latter affected by impedances of loading medium, polyurea coating, and metal substrate. Ackland et al. [45] manifested that the interfacial bonding strength between polyurea and metal layers markedly affected the permanent deformation of polyurea-metal bilayers subjected to explosions. By contrast, the micro-scale mechanisms of polyurea can be summarized as [46]: (i) shock wave-induced ordering [47], (ii) shock wave-induced crystallization/densification [47], (iii) breakage and generation of hydrogen bonds [48,49], and (iv) viscoelastic stress relaxation [46]. The mechanisms interrogated above at both macro and micro-scales are helpful for correctly using polyurea coating in engineering structures. To our knowledge, few published studies have focused on employing polyurea coating on all-metallic sandwich construction for blast/impact mitigation.

This paper proposes a novel shock-resistant corrugated core sandwich structure, by using polyurea-coated face sheets in lieu of traditional face sheets. According to our previous work [50,51], the existence of polyurea layer enables enhanced passive vibration attenuation of metallic corrugated core sandwich panels, due to substantial viscoelastic energy dissipation of the constrained polyurea layer. With pressing need for mitigating blast and impact damage, it is also of interest to investigate the shock resistance of such construction. The present study aims therefore to explore the effectiveness of polyurea coating on mitigating explosion/impact-induced deformation of metallic corrugated core sandwich panels and interrogate in detail the physical mechanisms by which polyurea coating accomplishes its mitigation effect. The study is expected to provide a new perspective to enhance the shock resistance of metallic sandwich construction.

2. Experimental investigation

Closed-cell aluminum foam projectiles are employed to dynamically load, via a light-gas gun, fully-clamped corrugated core sandwich panels with and without polyurea coating. Primary aims of the experimental investigation include:

(i) Compare the shock resistance of non-coated and coated corrugated sandwich panels;
(ii) Investigate the effect of relative position of polyurea coating on shock resistance;
(iii) Verify the fidelity of FE simulations on dynamic response.

Table 1
Geometric parameters of corrugated core sandwich panels studied (unit: mm).

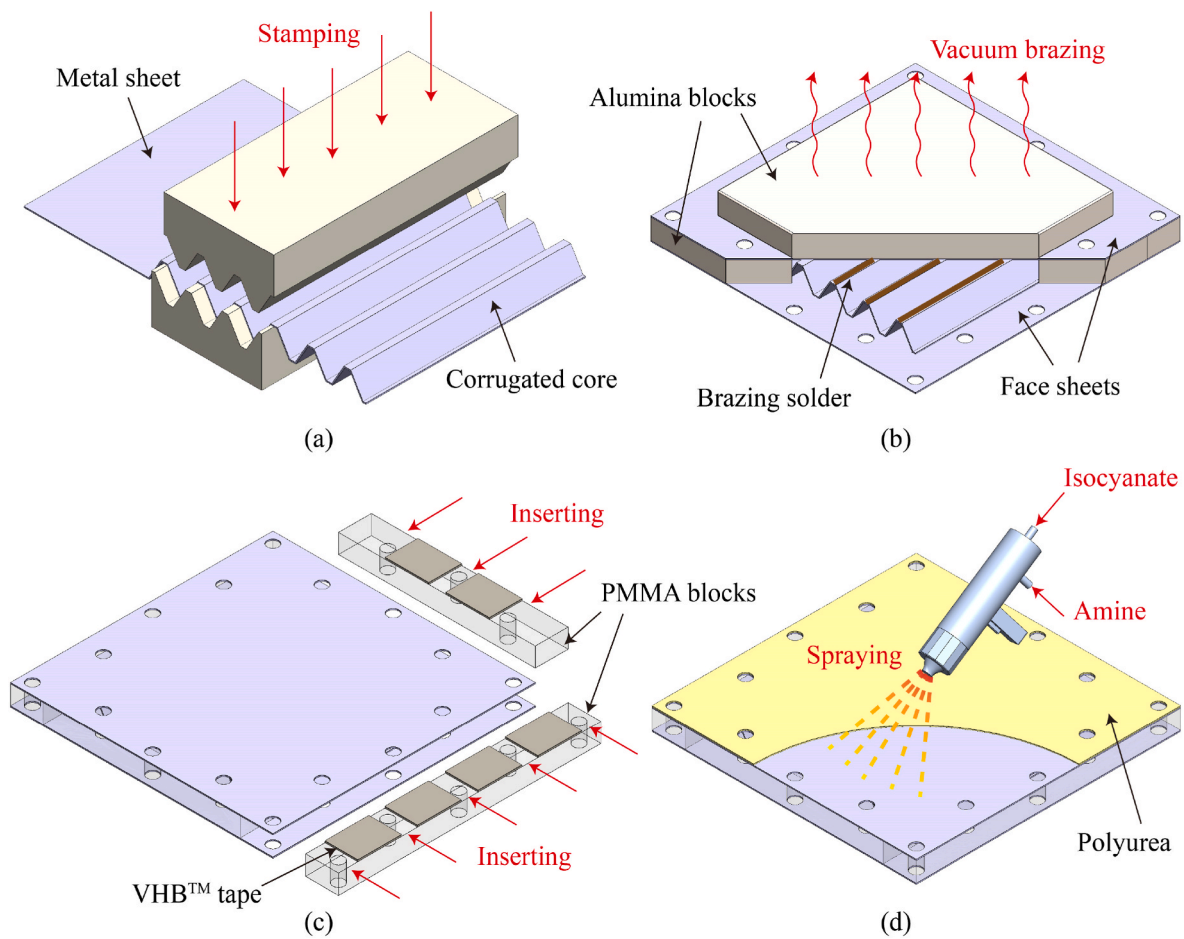| L	t_f	t_c	l_c	l_p	θ	L_b	d_b	$\bar{\rho}$
180	0.29	0.19	20	5	60°	30	10	1.81%

Fig. 2. Fabrication process of polyurea-coated corrugated core sandwich panel: (a) stamping, (b) brazing, (c) inserting, and (d) spraying.

2.1. Specimen configuration and manufacture

Fig. 1 presents the geometric configuration and representative volume element (RVE) of a square corrugated core sandwich panel tested in the current study, which encompasses two identical thin face sheets and a low-density trapezoidal corrugated core. For clarity, a global coordinate system (x, y, z) is introduced, where x, y and z- axis represent the longitudinal, transverse, and out-of-panel direction of corrugated core,

respectively. Relevant geometric parameters comprise length L and height H of sandwich panel; face sheet thickness t_f; core height H_c; length l_c, thickness t_c, and inclination angle θ of corrugation member; corrugation platform length l_p; PMMA insert length L_b; and bolt hole diameter d_b. The relative density of corrugated core, $\bar{\rho}$, can be expressed as:
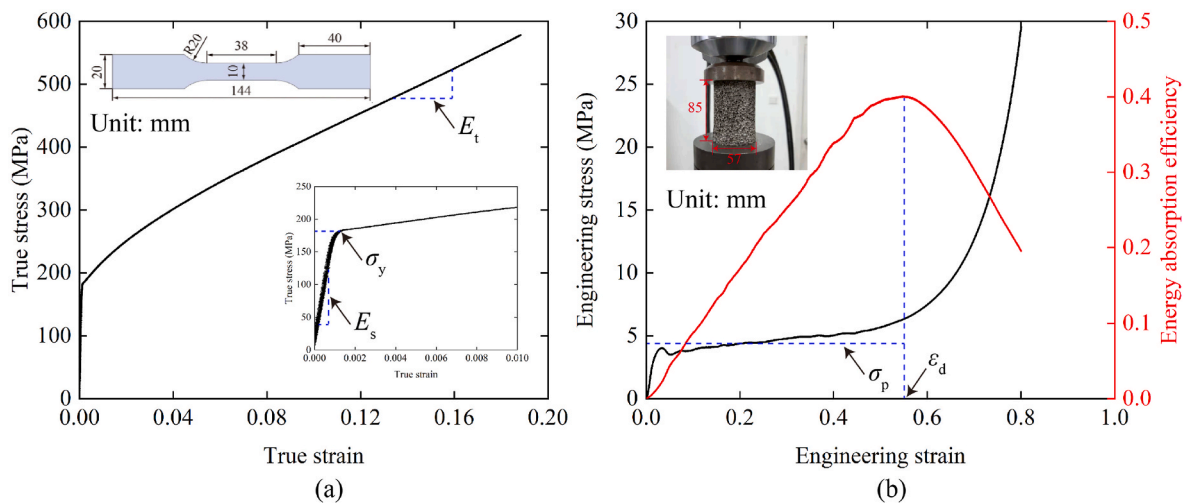

Fig. 3. (a) Quasi-static tensile true stress versus strain curve of 304 stainless steel, and (b) quasi-static compressive engineering stress versus strain curve of aluminum foam with closed cells.
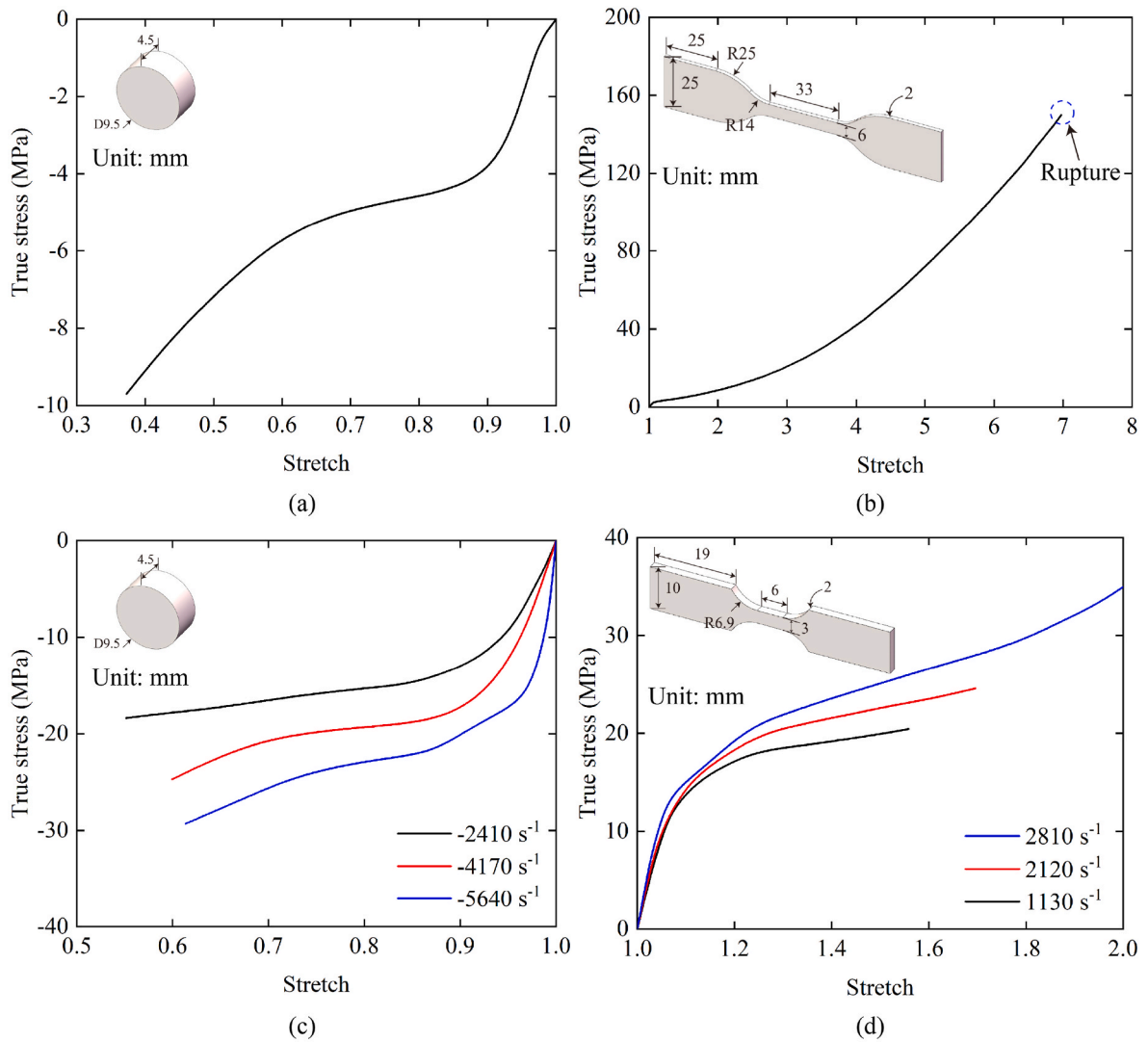
Fig. 4. Mechanical response of Qtech-420 polyurea elastomer under (a) quasi-static compression, (b) quasi-static tension, (c) dynamic compression, and (d) dynamic tension.
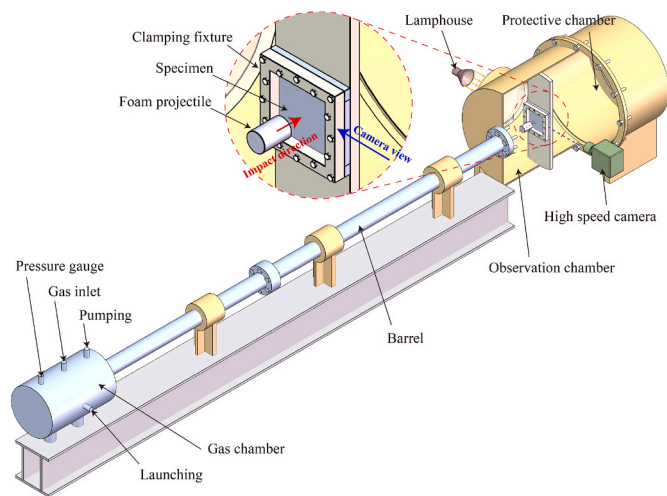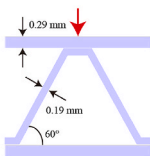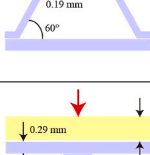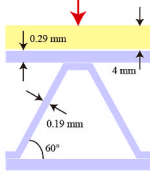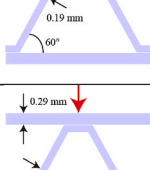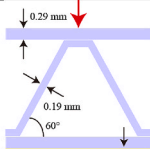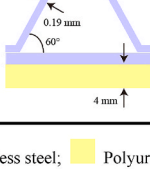

Fig. 5. Schematic diagram of the light-gas gun system used for foam projectile impact tests.

$$\overline{\rho} = \frac{t_c\left(l_p + l_c\right)}{\left(l_p + l_c \cos\theta\right)\left(t_c + l_c \sin\theta\right)} \tag{1}$$

Table 1 lists geometric parameters of the metallic corrugated core sandwich panels to be fabricated.

Fig. 2 shows the fabrication process of elastomer-coated metallic corrugated core sandwich panels. All sandwich panels are made of 304 stainless steel (supplied by Shanghai Haocheng Co., Ltd.). As with our previous efforts [25,26], metallic face sheets and corrugated core are assembled and bonded together via vacuum brazing. The brazing solder is prepared by mixing Ni76Cr14P10 alloy powder and oil-based adhesive (both supplied by Changsha Tianjiu Co., Ltd.) in a mass ratio of 8: 1. Each specimen is firstly heated to 640 °C at a rate of 8 °C/min and then held for 10 min to remove impurity gas (e.g., H_2, O_2, N_2, etc.). With a brazing temperature of 1040 °C adopted, the specimen is held for 15 min to let capillarity draw melting solder into brazing joints. After that, the furnace environment is gradually cooled down to room temperature at a rate of 16 °C/min. A few details of the fabrication process should be noticed: (i) The presence of corrugation platform provides a larger brazing area; (ii) Before heating, the furnace should be evacuated to 10^{-2} Pa or even lower; (iii) Proper pressure provided by alumina tiles facilitates a preferable solid-solution treatment, thereby leading to higher joint strength; (iv) Along the sides of each sandwich panel, drilled

Table 2
Summary of foam projectile impact tests.

Specimen No.	Configuration	m_s (g)	ρ_p (kg m^{-3})	v_0 (m s^{-1})	l_0 (mm)	I_0 (kPa s)	w_r (mm)
S-1		388.85	407.23	183	85	6.33	30.8
S-2		398.17	383.68	238	85	7.76	40.5
PS-1		583.87	371.63	205	85	6.48	25.5
PS-2		579.45	378.98	249	85	8.02	28.1
SP-1		581.76	370.14	202	85	6.36	26.5
SP-2		568.14	379.77	241	85	7.78	31.5

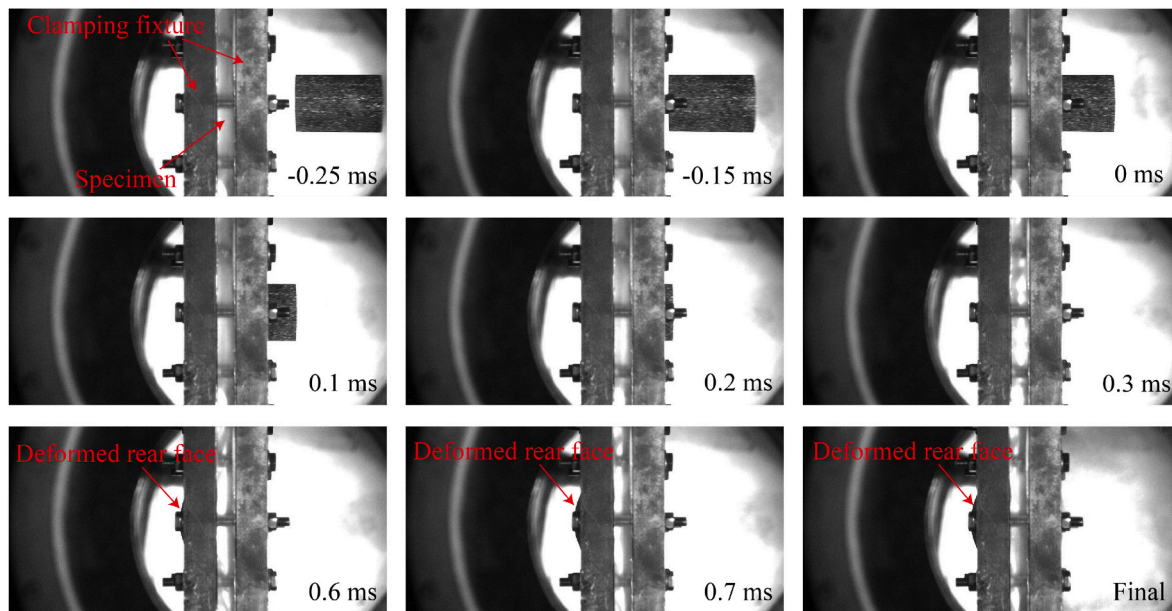■ 304 stainless steel; ■ Polyurea elastomer; → Impact direction

Fig. 6. Dynamic deformation process of specimen **S-2** at projectile momentum $I_0 = 7.76$ kPa s.

PMMA inserts are glued in the clamping area.

Qtech-420 polyurea elastomer (supplied by Qingdao Shamu Co., Ltd.) is spray-casted onto each sandwich panel uniformly. To discuss the effect of coating position, impact and rear faces are selected as the substrates to which polyurea elastomer adheres, respectively. After spraying, all samples are preserved at room temperature for two weeks, leading to higher strength and ductility of the polyurea. The polyurea is formed by condensation polymerization of difunctional isocyanates (OCN-R-NCO) and difunctional amines (H$_2$N-R′-NH$_2$) precursors. With the help of pre-applied primer, polyurea coating is tightly bonded with metal face sheets. Due to errors caused by manual operation, the thickness of polyurea coating on a single face sheet is measured to be 4 ± 0.2 mm.

2.2. Material characterization

Quasi-static uniaxial tensile tests at an engineering strain rate of 3.3 × 10^{-3} s^{-1} are conducted on 304 stainless steel. According to the standard ISO 6892–1:2009, dog-bone samples are cut from metal sheets that are subjected to the same brazing cycle described earlier. To
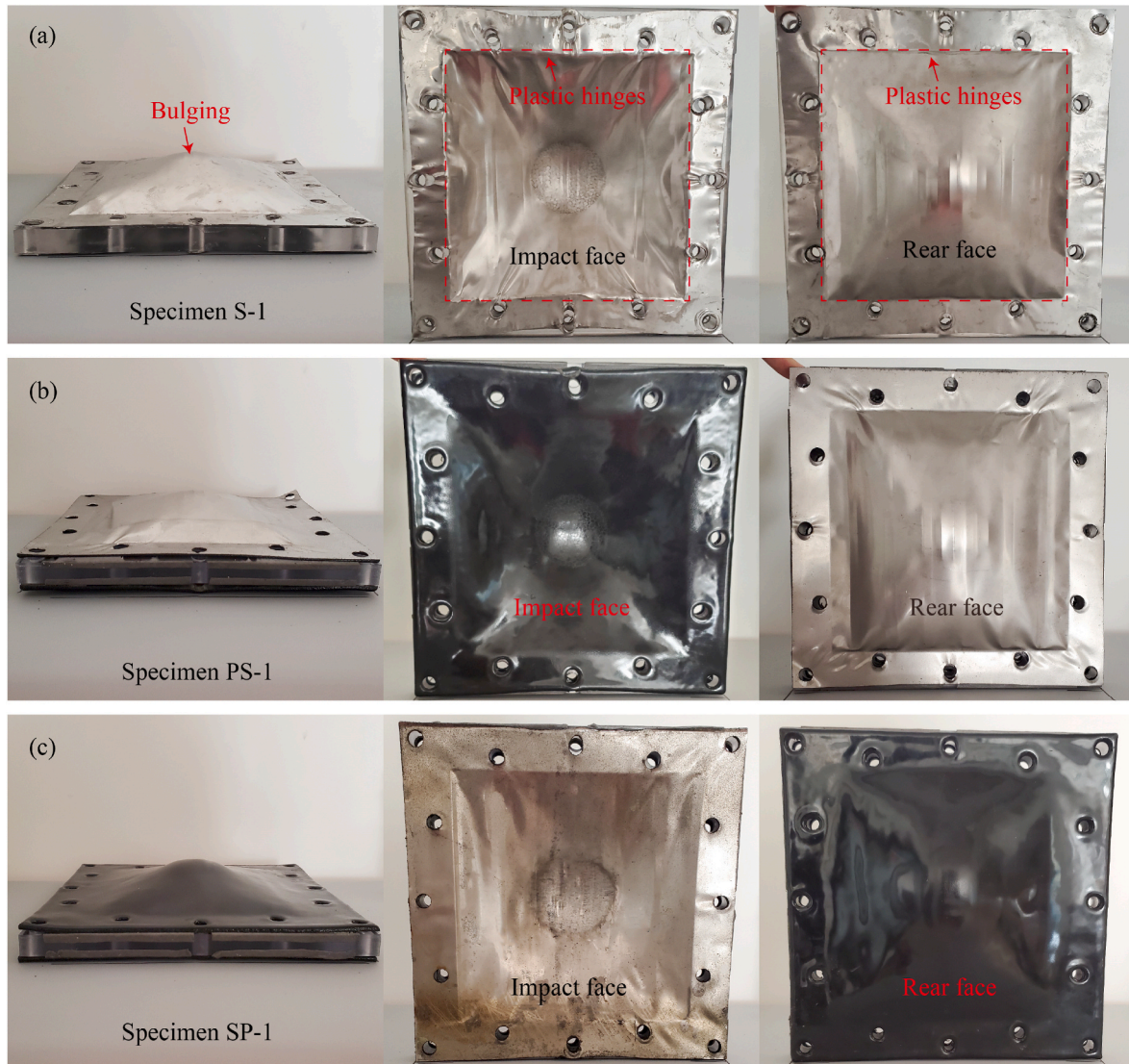
Fig. 7. Final deformed corrugated core sandwich panels with and without polyurea coating at average projectile momentum $I_0 \approx 6.39$ kPa s: (a) **S-1**, (b) **PS-1**, and (c) **SP-1**.

ascertain consistency, the tensile tests are conducted thrice, with average results taken as representative of material response. Fig. 3a plots the true stress versus strain curve of 304 stainless steel. Generally speaking, the material appears to be an elastic, linearly hardening solid, with density $\rho_s = 7800$ kg m^{-3}, Young's modulus $E_s = 200$ GPa, yield strength $\sigma_y = 180$ MPa, and tangent modulus $E_t = 1.8$ GPa.

Quasi-static uniaxial compression tests at an engineering strain rate of 1.0×10^{-3} s^{-1} are conducted on close-celled aluminum foam (density $\rho_f = 380$ kg m^{-3}). With reference to Andrews et al. [52], cylindrical samples with diameter of 57 mm and height of 85 mm are used to determine material response. Fig. 3b exhibits the engineering stress versus strain curve of the foam, from which the plateau stress is obtained as $\sigma_p = 4.8$ MPa. To estimate its densification strain ε_d, an energy efficiency parameter Λ is defined [53], as:

$$\Lambda(\varepsilon) = \frac{1}{\sigma(\varepsilon)} \int_0^\varepsilon \sigma(\varepsilon) d\varepsilon \qquad (2)$$

where the densification strain ε_d is determined via:

$$\left. \frac{d\Lambda(\varepsilon)}{d\varepsilon} \right|_{\varepsilon = \varepsilon_d} = 0 \qquad (3)$$

Accordingly, the metal foam specimen is densified at a strain of $\varepsilon_d = 0.55$, as shown in Fig. 3b.

Both quasi-static and dynamic compressive and tensile tests are performed on Qtech-420 polyurea elastomer (density $\rho_p = 950$ kg m^{-3}). The results are briefly introduced below, as more details can be found in a previous study [54]. Dog-bone samples are prepared for tensile tests in accordance with ISO 37:2017, while cylindrical samples are adopted for compressive tests with reference to ASM Handbook [55]. Fig. 4 displays the true stress versus stretch relations of polyurea under various strain rates. Note that positive and negative values of stresses/strain rates correspond to tensile and compressive stress states, respectively. Under quasi-static tension, the polyurea is able to elongate up to 700%, with an ultimate strength of 150 MPa, which indicates significant potential for blast and impact mitigation applications [41,42,56]. It has been elucidated that an effective impact-mitigating elastomeric coating should have both high strength and ductility [56], for an elastomeric coating with high strength but low ductility will fracture at small strains and spall off, curtailing its contribution to protection [41]. Also, it is observed that the mechanical response of polyurea is significantly rate-dependent due to viscoelasticity.
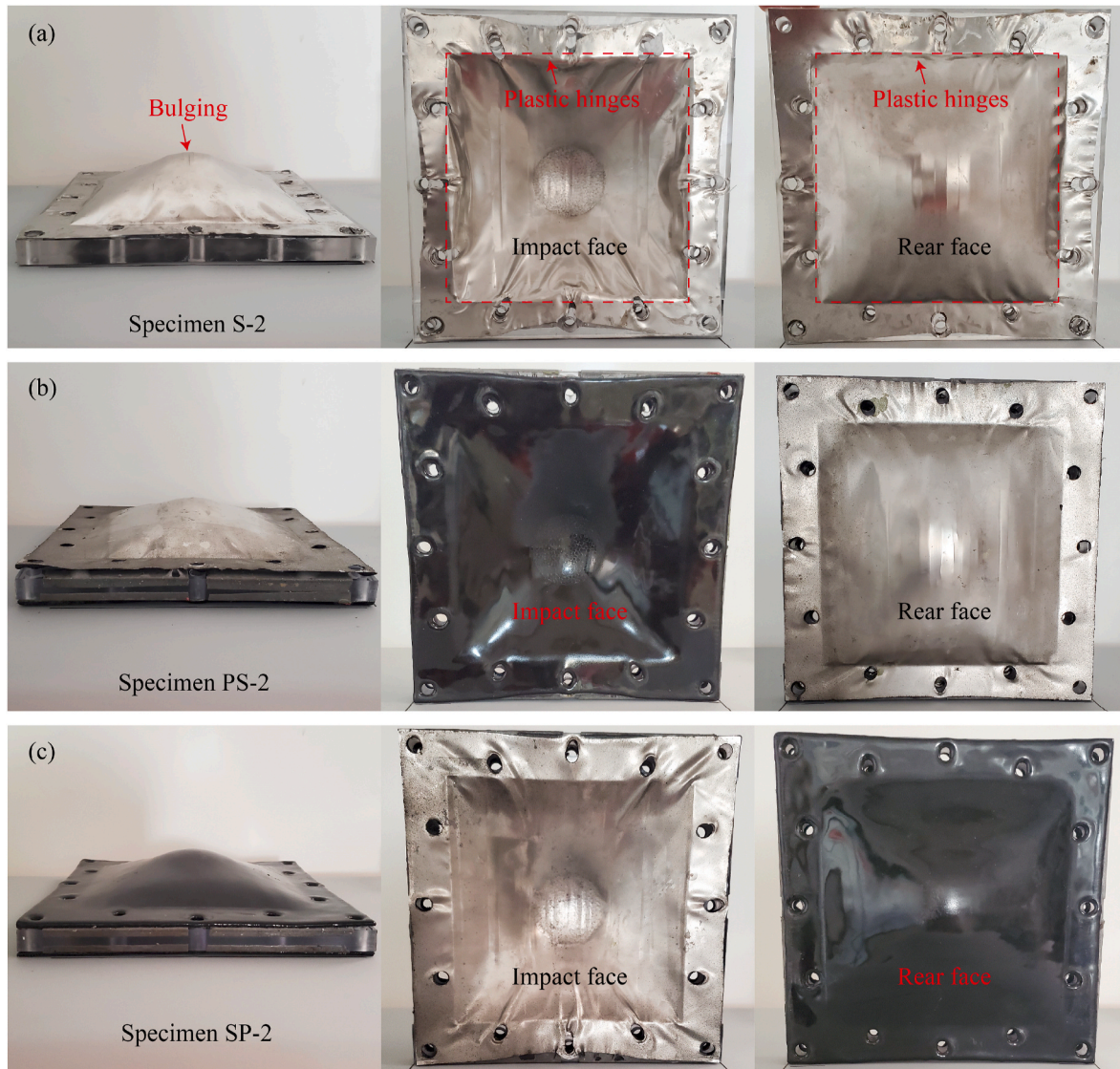
Fig. 8. Final deformed corrugated core sandwich panels with and without polyurea coating at average projectile momentum $I_0 \approx 7.85$ kPa s: (a) **S-2**, (b) **PS-2**, and (c) **SP-2**.

2.3. Foam projectile impact tests

The use of close-celled aluminum foam projectiles to simulate shock loading on edge-clamped samples is employed, which is able to generate well-characterized pressure-time histories representative of shock loading caused by air and underwater explosions [57]. The initial projectile momentum per unit area I_0 can be defined by:

$$I_0 = \rho_f l_0 v_0 \tag{4}$$

where ρ_f, l_0, and v_0 are the density, length, and velocity of foam projectile, respectively. The impulse per unit area imparted on the structure can be approximated by the projectile momentum if the mass ratio η and strength ratio φ is very close to zero [12].

$$\eta = \frac{M_p}{M_s} \tag{5}$$

$$\varphi = \frac{\sigma_y \varepsilon_d}{\rho_f v_0^2} \tag{6}$$

where M_p and M_s are the mass of the foam projectile and structure; σ_y, ε_d and ρ_f are the yield stress, densification strain, and mass density of the

foam projectile. In practice, it is sometimes hard to satisfy the above requirement; therefore, we suggest that these two ratios should be at least smaller than 0.2. As shown in Fig. 5, the light-gas gun system encompasses a gas chamber, barrel, and protective chamber. The length, outer diameter, and inner diameter of the barrel are 5 m, 135 mm, and 57 mm, respectively. The specimen is bolted down to a rigid fixture by sixteen M10 bolts, while the fixture is welded to the observation chamber. Cylindrical foam projectiles with length $l_0 = 85$ mm and diameter $d_0 = 57$ mm are electro-discharge machined from close-celled aluminum foam (supplied by Anhui Yiming Co., Ltd.). The barrel is aligned with the center of the clamped sandwich panel to ensure a central impact of foam projectile. To prevent tumbling, the length-diameter ratio of the projectile should fall within the range of 0.82~1.75 [12]. The dynamic deformation process of each specimen is recorded using a high-speed camera (I-SPEED 713, IX), with inter-frame time of 50 μs, exposure time of 5 μs, and resolution of 899 × 444 pix. For accuracy, the impact velocity v_0 at each test is calculated by using motion analysis software (ProAnalyst, Xcitex). After the impact test, the deformed sandwich panel is removed from the fixture and examined to observe deformation and failure modes. Permanent deflections of rear face sheets are also measured using a laser displacement sensor

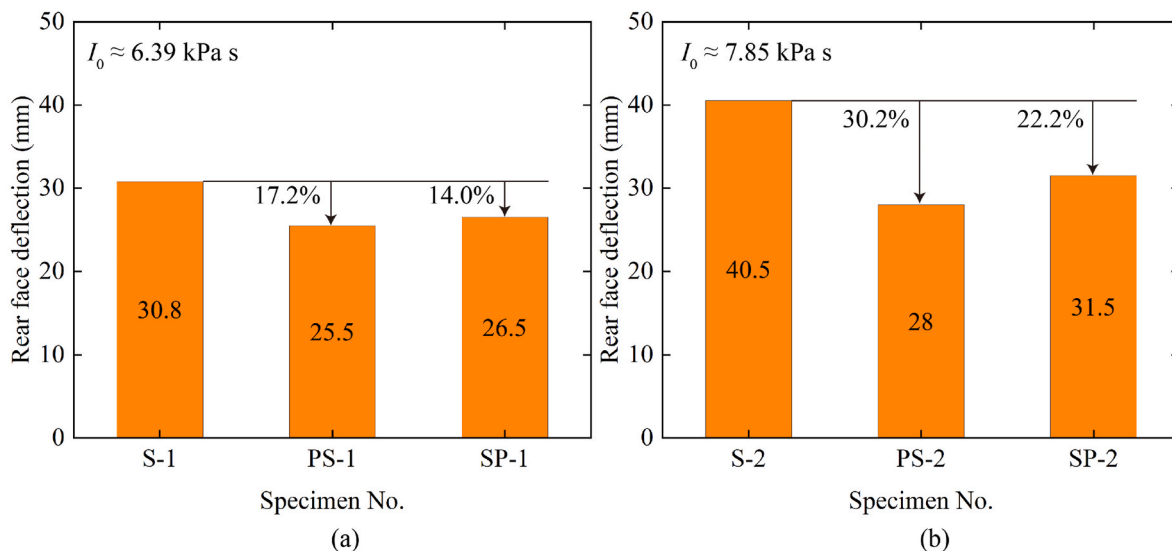**Fig. 9.** Comparison of permanent mid-span deflection of rear face for corrugated core sandwich panels with and without polyurea coating at: (a) $I_0 \approx 6.39$ kPa s, and (b) $I_0 \approx 7.85$ kPa s.
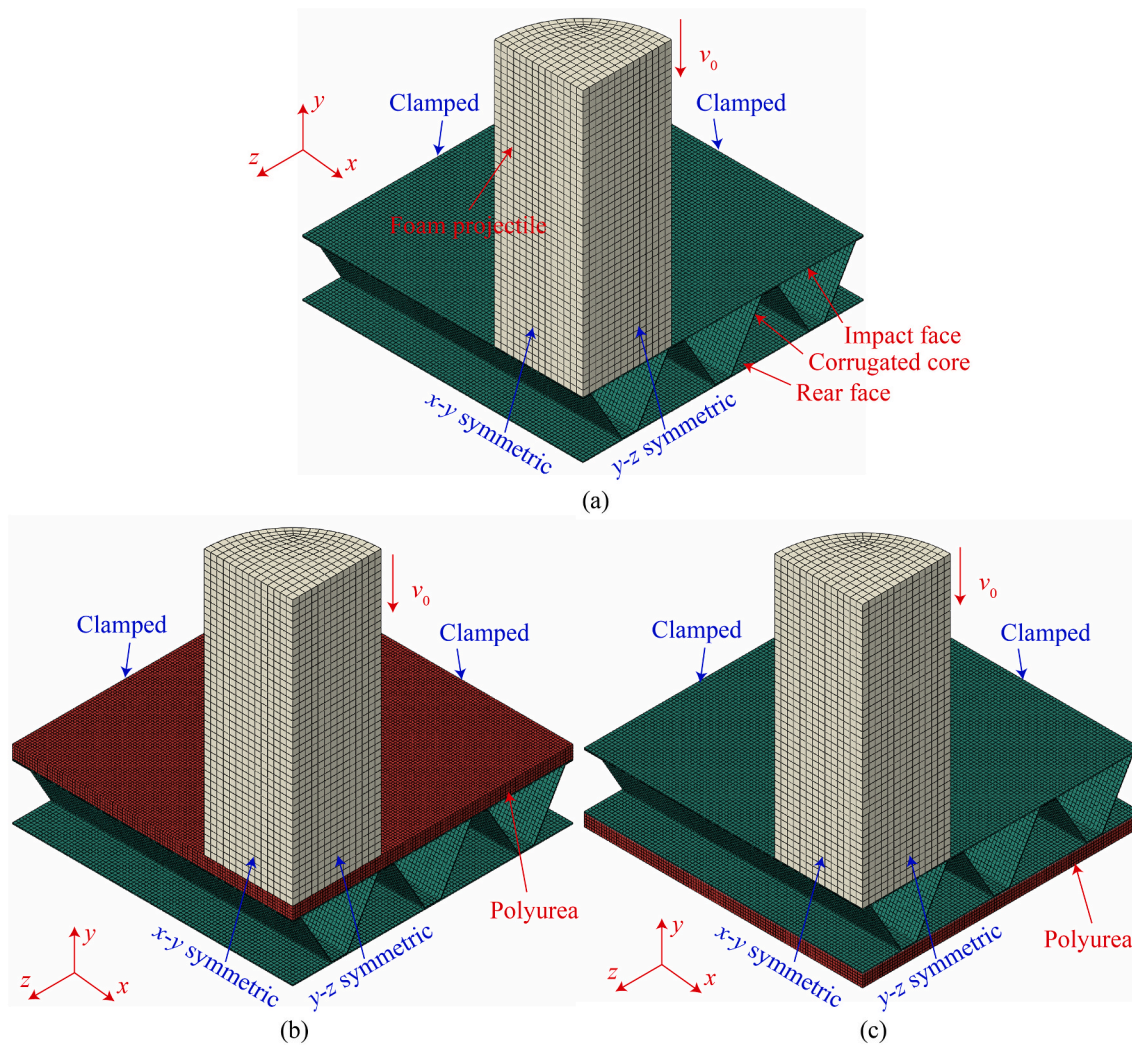

Fig. 10. Finite element models of one-quarter corrugated sandwiches: (a) without polyurea coating, (b) with polyurea coating on impact face, and (c) with polyurea coating on rear face.
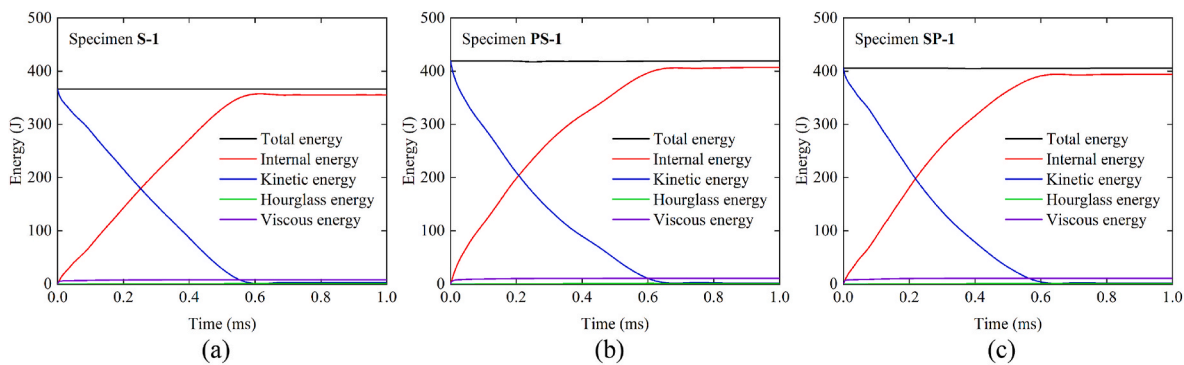
Fig. 11. Numerically predicted energy histories for (a) **S-1**, (b) **PS-1**, and (c) **SP-1**.
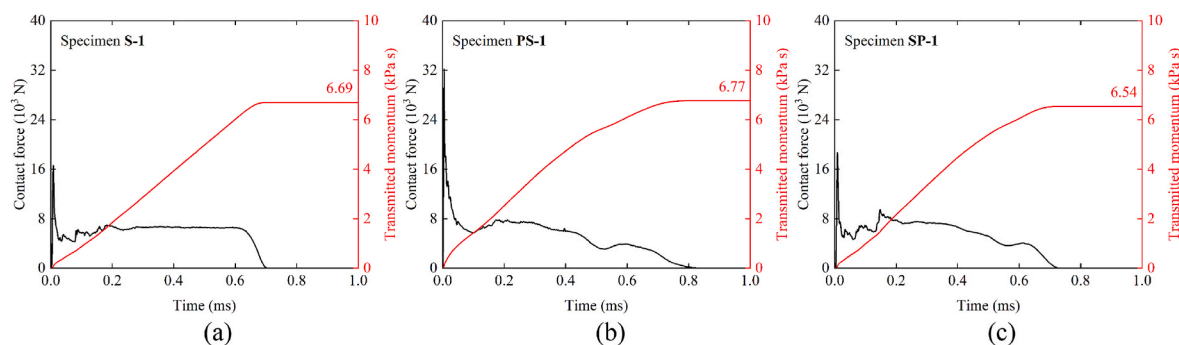

Fig. 12. Numerically predicted histories of contact force between foam projectile and impact face and the corresponding transmitted momentum histories for (a) **S-1**, (b) **PS-1**, and (c) **SP-1**.
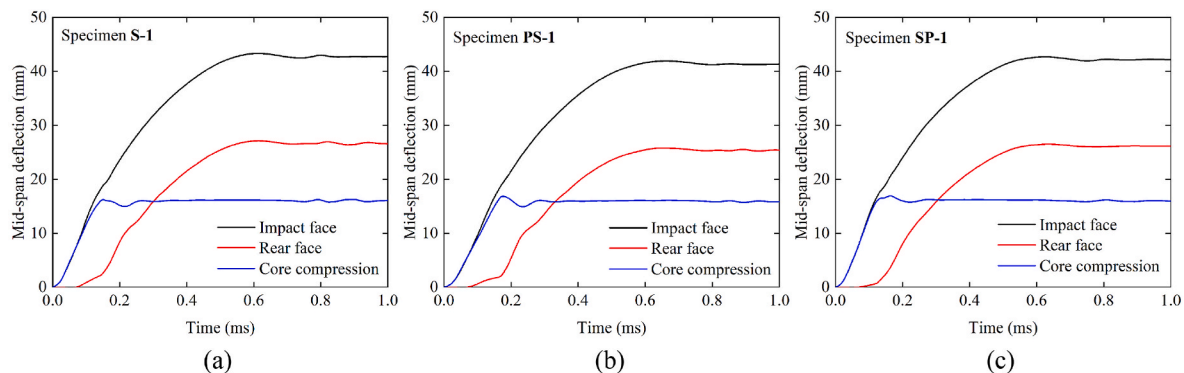

Fig. 13. Numerically predicted mid-span deflection histories for (a) **S-1**, (b) **PS-1**, and (c) **SP-1**.

(optoNCDT2300, Micro-Epsilon) and employed to compare the shock resistance of specimens with and without polyurea coating.

3. Experimental results

Two selected levels of metal foam projectile momentum are applied to sandwich panels, with or without polyurea coating. The parameters of foam projectiles used in the tests and the corresponding measured deflections are summarized in Table 2. All specimens are impacted at their brazing joints (the effect of impact position is discussed in Appendix B). Three aspects of experimental observations are manifested in this section, including dynamic deformation process via high-speed photography, deformation/failure modes via post-mortem analysis, and mid-span deflection of rear face measured from post-impact samples. For clarity, let the face sheet impacted by foam projectile as impact face and the other one as rear face, respectively. Further, three abbreviations (i.

e., **S**, **PS**, and **SP**) are adopted to represent separately non-coated, impact-side coated, and rear-side coated corrugated core sandwich panels. Recall that ρ_p, v_0, and l_0 represent the density, velocity, and length of foam projectile, respectively. m_s represents specimen weight, while w_r denotes mid-span permanent deflection of rear face.

3.1. Dynamic deformation process

Following our previous analysis of all-metallic sandwich beams [25, 26], the dynamic deformation process of a clamped sandwich panel subjected to foam projectile impact loading is approximately decoupled into four stages, as [24]: (i) the projectile momentum is transferred to the panel so that the impact face obtains an initial velocity; (ii) as the corrugated core starts to be compressed, the impact face decelerates while the rear face accelerates, which ends with both faces approaching the same velocity; (iii) both the face sheets and the crushed core move
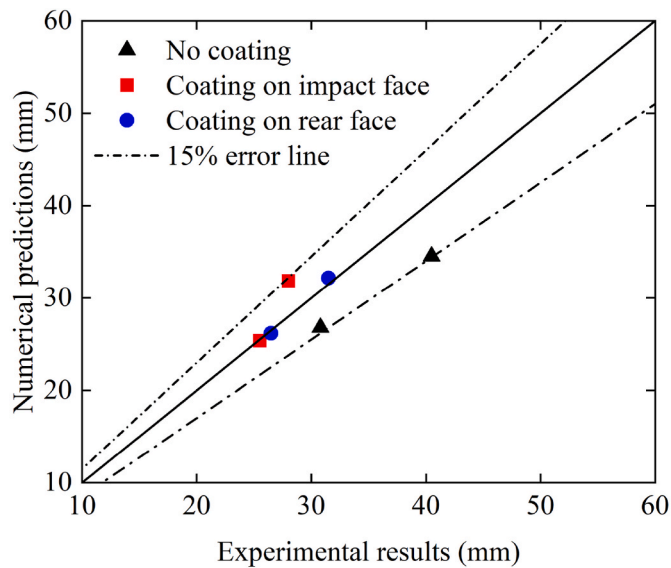
Fig. 14. Comparison between experimental and numerical results of mid-span rear face deflections.

together until the sandwich comes to rest at the point of maximum mid-span deflection, causing overall deformation of combined plastic bending and longitudinal stretching; (iv) elastic oscillation occurs, with mid-span deflections of both faces fluctuating within a small amplitude and eventually approaching steady-state values. Similar dynamic responses are observed in the current impact tests on both non-coated and coated specimens. As each specimen is mounted on the clamping fixture with a thickness of 30 mm, the high-speed photographic images can only capture very little of the structural deformation unless the rear face deflection is more than 30 mm. For instance, Fig. 6 displays the dynamic deformation process of non-coated specimen **S-2** impacted by a foam projectile with initial momentum $I_0 = 7.76$ kPa s. It is manifested that the deformed rear face appears in the image at 0.6 ms, and its deflection keeps constant at around 0.7 ms. For clamped plate structures, more details of their deformation process can be seen in the numerical simulation section (Fig. 15).

3.2. Deformation/failure modes

According to previous studies [58,59], the deformation and failure modes of all-metallic corrugated core sandwich panels subjected to blast loading are identified into four primary mechanisms: (i) Mode I - large inelastic deformation; (ii) Mode II - partial tearing at central area; (iii) Mode III - complete tearing at central area; (iv) Mode IV - petalling at central area. It has been ascertained that the appearance of such deformation and failure modes is related to geometric configuration of sandwich panel, level of blast/impact loading, effective area of applied loading, and the like [58]. Upon these definitions, a post-mortem analysis on final deformed specimens in the current study is carried out.

Figs. 7 and 8 compare the deformation and failure models of non-coated and coated sandwich panels, impacted at two different projectile momentum. For all specimens tested, the deformation mechanism is dominated by large inelastic deformation (Mode I). For non-coated sandwich panels (Figs. 7a and 8a), as the projectile momentum is imparted on the sandwich over a circular loading patch, plastic hinges initiate around the edge of foam projectile and then move towards the central region and clamped edge of the sandwich. Eventually, stationary plastic hinge lines are observed on both the impact and rear faces near the clamping boundary. As projectile momentum is increased, bulging is observed on rear face, leading to large overall inelastic deformation of the sandwich. Note that no crack is observed on either the impact or rear

face. Besides, it is seen that pull-in of both faces results in severe shear failure around the bolt holes (Fig. 8a). By contrast, the presence of polyurea coating reduces bulging deformation in the central area and eliminates shear deformation around bolt holes (Fig. 7b ~ c and 8b ~ c). Due to the outstanding ductility and adhesiveness of as-used polyurea, the dynamically loaded coating remains perfectly bonded with metal face sheets and maintains intact with no crack appearing on its surface. However, it should be noticed that polyurea coating with low ductility may fracture at small strain and spall off, curtailing its contribution to protection [56,60].

3.3. Quantitative results

To quantitatively testify the mitigation effect of polyurea coating, Fig. 9 compares the mid-span rear face deflections of corrugated core sandwiches for two selected projectile momentum. The presence of polyurea coating is able to curtail the rear face deflection, but the level of benefit is seen to be dependent upon coating position and projectile momentum. In addition, the deformations of impact-side coated specimens are smaller than that of rear-side coated ones. Similar to existing results [61], better blast resistance of sandwich panels can be achieved by replacing identical front and rear face sheets with asymmetric ones. Specifically, the design scenario of a thick impact face and a thin rear face is preferred for blast-resistant sandwich construction. Similarly, impact-side coating strengthens the impact face, causing asymmetry of both face sheets. Additionally, with the increase of impact momentum, the boundary effect is observed to be more serious for non-coated panels. The shear failure of face sheets around bolt holes is significantly prohibited by polyurea coating, thus enhancing the level of its benefit on mitigating rear face deflection.

4. Numerical predictions

The commercially available FE code Abaqus/Explicit v2020 is utilized to conduct numerical simulations on both non-coated and coated sandwich panels under foam projectile impact. In addition to structural deformation (as mentioned in Section 3), some fundamental results that are not available from the experiments are analyzed in this section, such as momentum transfer and energy absorption. These clues enable more elaborated elucidation of the physical mechanisms underlying the mitigation role of polyurea coating.

4.1. Model description

FE models of one-quarter corrugated sandwich structures with and without polyurea coating are presented in Fig. 10. For each type of sandwich, both the face sheets and corrugated core are meshed using four-node general-purpose shell elements with reduced integration (S4R in Abaqus nomenclature), with a grid size of 1 mm adopted. For accuracy, five integration points along shell element thickness are employed. Eight-node brick elements with reduced integration (C3D8R in Abaqus nomenclature) are used to discretize metal foam projectiles and polyurea coating, with a grid size of 2 mm and 0.8 mm accepted, respectively. General contact is applied to all components of the sandwich structure. With reference to experimental observations, the corrugated core is assumed to be perfectly bonded with face sheets using a tie contact option. The same contact algorithm is set for the interface between polyurea coating and face sheet. To improve computational efficiency, two symmetric boundary conditions are employed for each one-quarter model. All freedom of degrees, including displacements and rotations, are constrained at the clamping edges of each specimen. To eliminate element distortion and ensure energy balance of FE simulation, the control of hourglass energy is activated using the relaxed stiffness method. Geometric configurations of the numerical models and initial velocities of the metal foam projectiles are based on Table 2. Last but not least, constitutive relations used in the current simulations can
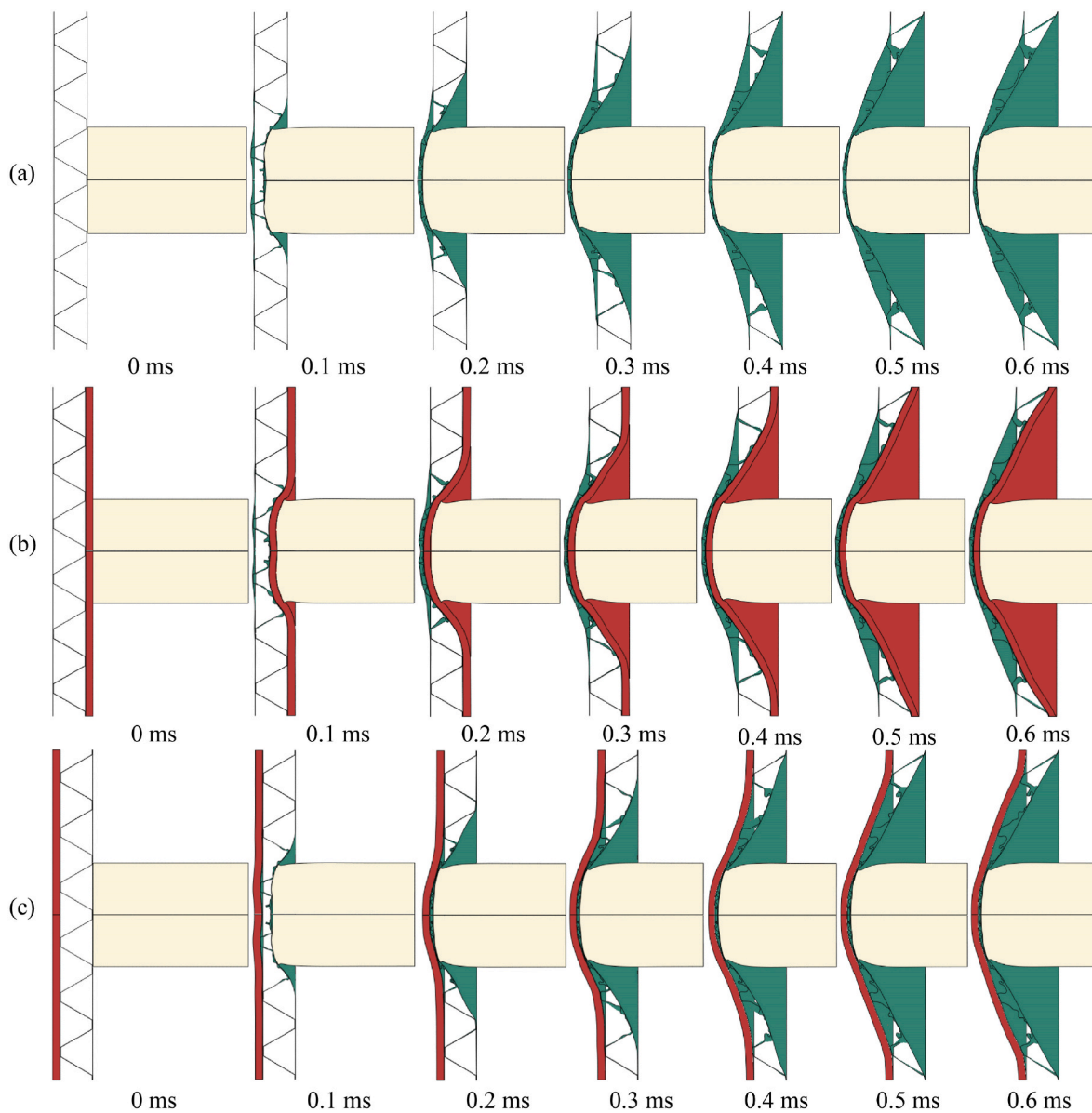
Fig. 15. Numerical predicted deformation process for (a) **S-1**, (b) **PS-1**, and (c) **SP-1**.

be seen in Appendix A.

4.2. Validation work

First and foremost, the energy conservation of each simulation should be checked for the correctness of FE simulation results. To this end, Fig. 11 presents the numerically predicted energy versus time histories of non-coated and coated specimens, i.e., **S-1**, **PS-1**, and **SP-1**, respectively. It is ascertained that, at any time after foam projectile impact, the sum of kinetic energy, internal energy, hourglass energy, and viscous energy is equal to the total energy of the whole system. The hourglass energy is usually caused by excessive deformation and distortional of elements with reduced integration, while introducing bulk viscosity aims to curtail stable time increment and control high-frequency oscillations. According to the convention of Abaqus [62], a widely accepted tolerance is that hourglass energy needs to be limited to 10% of total energy, while viscous energy is less than 10% of internal energy. It is testified that the results of Fig. 11 strictly meet this standard of energy balance, thus indicating the prediction accuracy of the present FE models.

Consider next the momentum of foam projectile that is transferred to the dynamically loaded sandwich. Fig. 12 presents the history of contact force imparted on the impact face, for both non-coated and coated sandwiches. When the impact face is struck by foam projectile, the contact force between impact face and projectile increases sharply from zero to a peak, then undergoes a sudden drop and eventually vanishes. It is manifested that the peak force of the impact-side coated specimen **PS-1** is relatively higher than that of the other two specimens, **S-1** and **SP-1**. Then, to analyze momentum transfer on the contact interface, the transmitted momentum per unit area I_t is calculated as:

$$I_t = \frac{\int_0^{t_c} F_c dt}{A_c} \tag{7}$$

where F_c, t_c and A_c is the contact force, period, and area, respectively. Fig. 12 also displays the numerical predicted transmitted momentum histories of the three specimens considered. It is seen that the transmitted momentum for non-coated and coated sandwiches is approximately the same and equal to their initial projectile momentum (listed in Table 2).

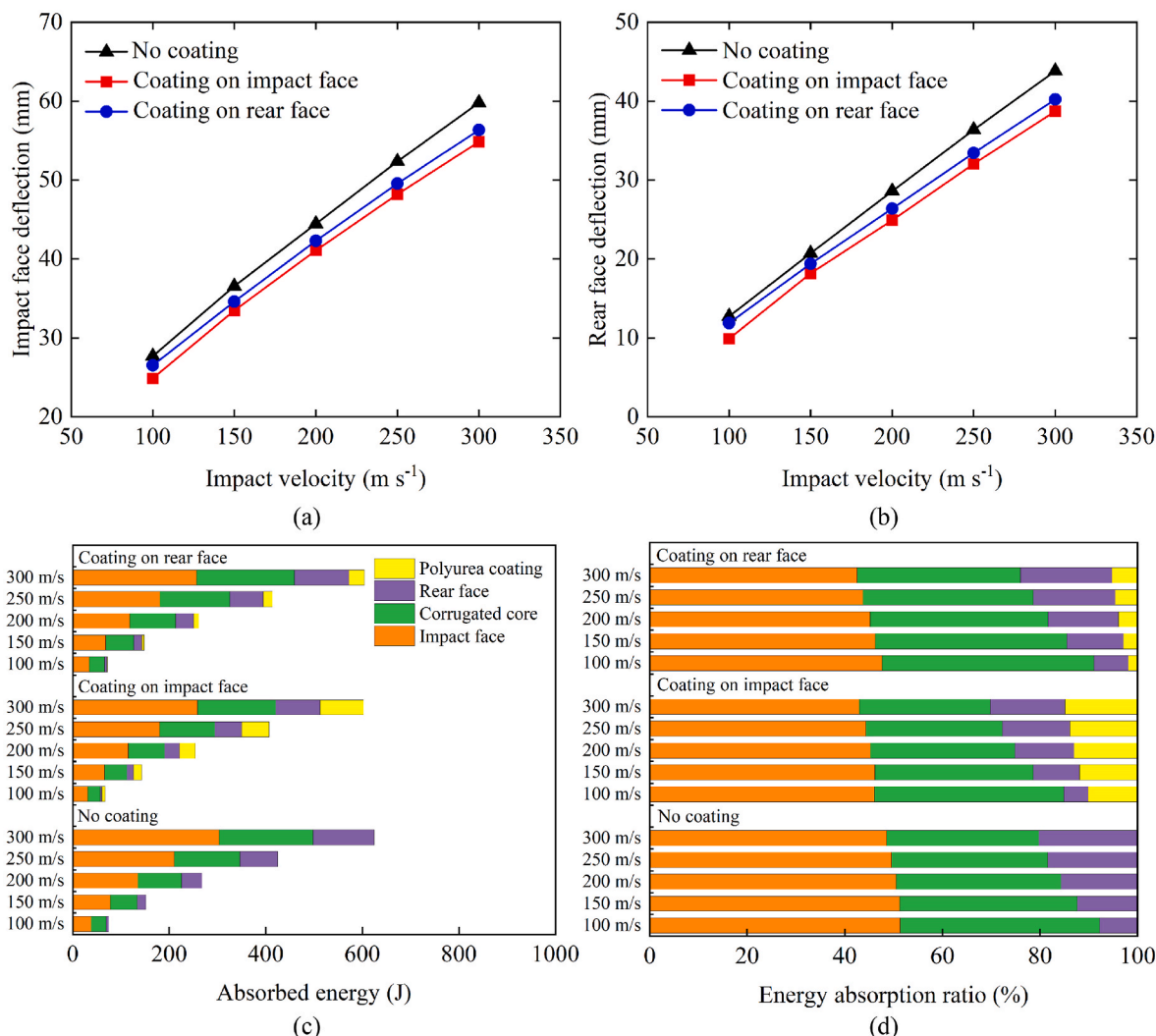Fig. 13 exhibits the numerically predicted mid-span deflection versus

Fig. 16. Shock resistance as a function of impact velocity: mid-span permanent deflection of (a) impact face and (b) rear face, and (c) absorbed energy and (d) energy absorption ratio of each sandwich component.

time curves of both impact and rear faces for specimens **S-1**, **PS-1**, and **SP-1**. For each specimen, the corresponding core compression is obtained by subtracting rear face deflection from impact face deflection. Permanent deflection is estimated by averaging the displacements over several cycles of elastic oscillations (from trough to peak) immediately after the peak displacement. As shown in Fig. 14, there is reasonable agreement between the measured and predicted rear face deflections at mid-span, for both non-coated and coated specimens. However, some discrepancies exist though the maximum difference is less than 15%. The difference may be attributed to the following factors. Firstly, perfectly clamping boundary condition assumed in FE simulations is not fully representative of experimental situation. It is observed experimentally that the pull-in of face sheets leads to severe shear deformation around bolt holes, especially for non-coated specimens (Fig. 8a) at relatively high projectile momentum. Secondly, manufacturing defects in factual specimens are not considered in FE simulation models. Given that the face sheets and corrugated cores are made of thin metal sheets (Table 1), vacuum brazing may cause undesirable thermal deformation of sandwich components. Thirdly, the face sheets and corrugated core are tied together in each specimen, with no debonding considered in FE simulations.

The simulated dynamic deformation evolutions of non-coated and coated sandwich panels are displayed in Fig. 15, with the time labeled on each graph taken with reference to the instant of shock loading

commencement. The impact and rear face deflections can be seen in the above displacement histories (Fig. 13). As the peak displacement is reached at around 0.6 ms, we just showcase the predicted deformation process between 0 and 0.6 ms. Similar to previous observations [25,26], the corrugated core from the central to clamping region exhibits different levels of crushing, and overall bending and stretching deformation of the face sheets are captured. The different deformation mechanisms of face sheets and corrugated core determine their distinct contribution to shock resistance of sandwich construction.

4.3. Discussions

Thus far, the enhanced shock resistance of the proposed polyurea-strengthened metallic corrugated core sandwich panels has been ascertained. Polyurea coating can effectively mitigate overall deformation at mid-span and eliminate shear deformation around bolts holes of the clamping fixture. There is good agreement between experimental measurements and numerical predictions on the dynamic response, deformation modes, and permanent deformations, for both non-coated and coated specimens. In this section, the high-fidelity FE models established are employed to quantify the effects of impact velocity, coating thickness, coating area, and coating position on the shock resistance of polyurea-coated sandwich panels, with particular focus placed upon the permanent deflections of both face sheets and energy
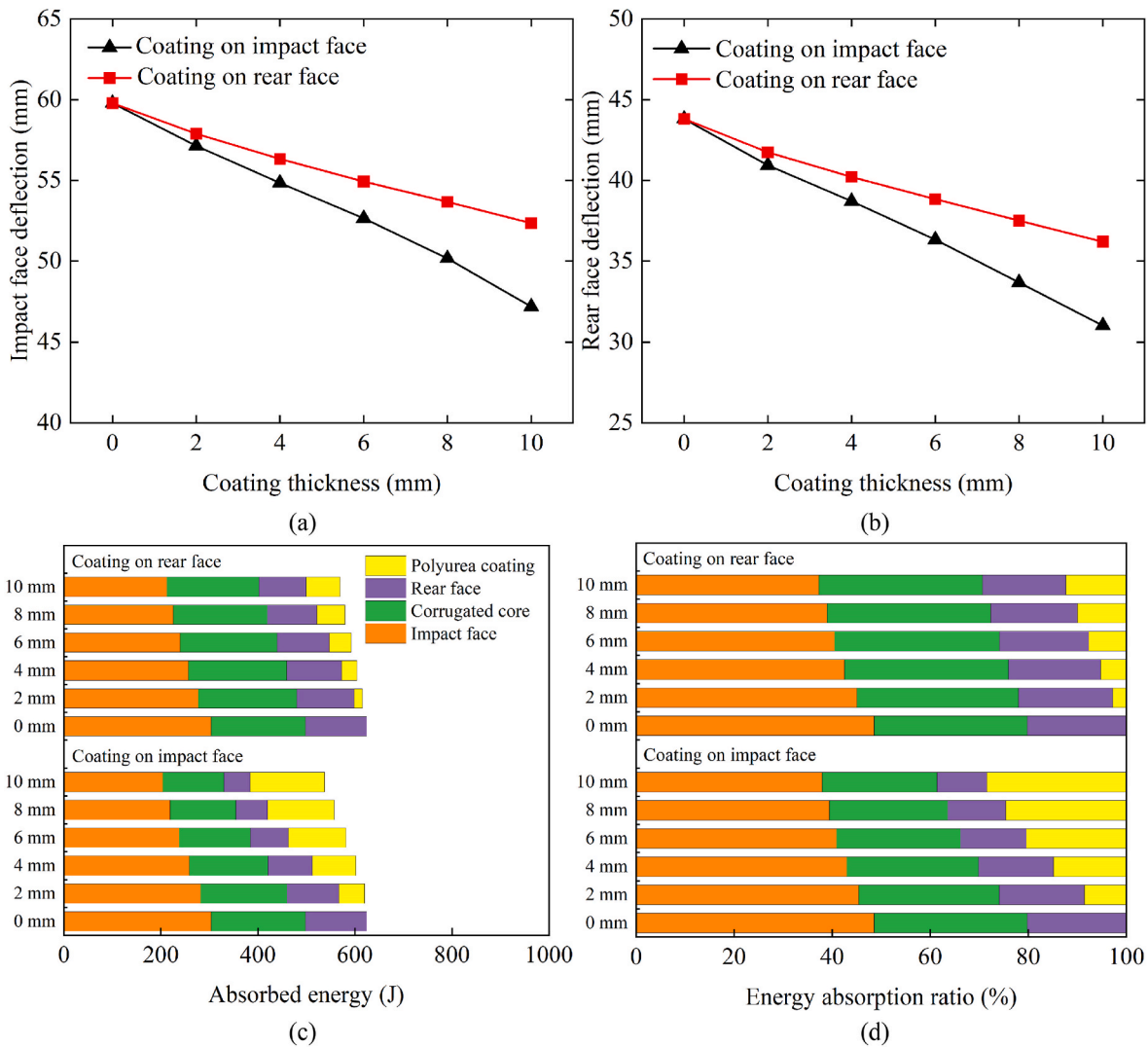
Fig. 17. Shock resistance as a function of coating thickness: mid-span permanent deflection of (a) impact face and (b) rear face, and (c) absorbed energy and (d) energy absorption ratio of each sandwich component.

absorption of sandwich components. The boundary effect observed in the tests is ignored. The aim is to interrogate the mechanisms of polyurea reinforcing by which it achieves the mitigation effect on impact deformation.

4.3.1. Effect of impact velocity

Consider first impact velocity affects the level of benefit of polyurea coating on mitigating impact deformation. Five different impact velocities, 100, 150, 200, 250, and 300 m s^{-1}, of foam projectiles with an identical density of 380 kg m^{-3} are dynamically imparted on non-coated, impact-side coated, and rear-side coated sandwich panels, respectively. Based on Eq. (4), the corresponding initial projectile momentum per unit area is obtained as 3.2, 4.8, 6.5, 8.1, and 9.7 kPa s. The thickness of polyurea coating is set as 4 mm, and the geometric parameters of sandwich panels are consistent with experimental tests (listed in Table 1).

Fig. 16a ~ b show the impact and rear face deflections at mid-span for non-coated and coated panels. With the increase of projectile momentum, combined bending and stretching lead to larger permanent deformation of the panels [24]. At different levels of deformation, the reinforcing of polyurea coating is capable of curtailing the permanent deflections of both impact and rear faces at mid-span. Relative to non-coated panels, the reduction of rear face deflection for impact-side

coated panels maintains a stable level (~12%). As with previous observations of Fig. 9, the position of polyurea coating dictates its effectiveness for mitigating impact deformation. At the selected projectile momentum, the impact-side coated panels exhibit superior shock resistance relative to the rear-side coated ones. The absorbed energy and energy absorption ratio of each sandwich component are presented in Fig. 16c ~ d. For non-coated panels, the impact faces acquire larger plastic strain energies than those of the rear faces and corrugated cores. By contrast, the presence of polyurea coating curtails the plastic strain energy stored in a sandwich panel, thus causing relatively small deformation. Further, a polyurea coating placed on the impact face dissipates much more shock energy than that on the rear face. Another interesting finding is that the contribution of polyurea coating to energy absorption increases gradually with the increase of projectile momentum.

4.3.2. Effect of coating thickness

To quantify the effect of coating thickness on the impact mitigation role of polyurea coating, polyurea coating with varying thicknesses (i.e., 2, 4, 6, 8, and 10 mm) is applied to either the impact or rear face. For consistency, the impact velocity of foam projectile with density of 380 kg m^{-3} is set as 300 m s^{-1}, corresponding to a projectile momentum per unit area of 9.7 kPa s.

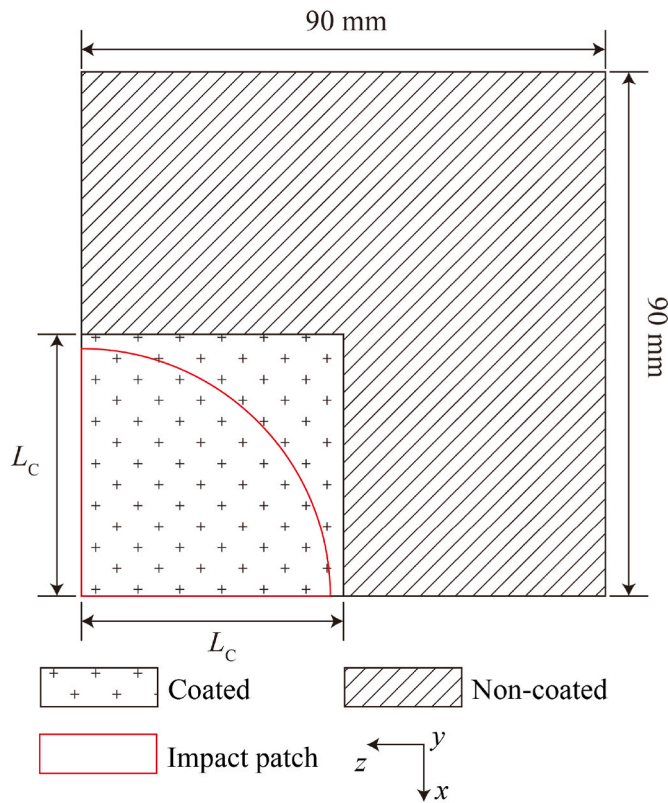Fig. 17a ~ b plot the impact and rear face deflections at mid-span as

Fig. 18. Illustration of non-coated and coated area of a one-quarter face sheet. (Global coordinate used here is consistent with that used in finite element model.)

functions of coating thickness. As the coating thickness increases, both the impact and rear face deflections decrease. However, similar to the finding of Section 4.4.1, the shock resistance of impact-side coated panels is much better than that of rear-side coated ones, irrespective of coating thickness. Compared with non-coated panels, the reduction of rear face deflection for panels retrofitted with 10 mm coating on the impact face is 29%, while that for panels with the same coating on the rear face is 17%. Fig. 17**c** ~ **d** display the absorbed energy and energy absorption ratio of each sandwich component. The contribution of polyurea coating to shock energy dissipation is elevated as its thickness increases. The superior shock resistance of impact-side coated panels is somewhat attributed to the higher energy absorption ratio of polyurea coating in the whole sandwich construction.

4.3.3. Effect of coating area
In this sub-section, the influence of coating area is discussed. In the experiments, specimens with polyurea coating applied to the entire face sheets are tested. In practice, it might be more cost-efficient to spray-cast polyurea elastomer on the central region of the face sheet where its plastic deformation is the largest. It is therefore of interest to explore the design scenario of partial polyurea coating with length L_c, as illustrated in Fig. 18. Accordingly, the coating area ratio can be expressed as:

$$\text{Area ratio} = \frac{L_c^2}{90 \times 90 \text{ mm}^2} \tag{8}$$

Upon setting the coating length as 40.2, 56.9, 69.7, 80.5, and 90 mm, five different area ratios (i.e., 0.2, 0.4, 0.6, 0.8, and 1) are selected. For consistency, the impact velocity of foam projectile (density fixed at 380 kg m^{-3}) is set as 300 m s^{-1}, corresponding to a projectile momentum per unit area of 9.7 kPa s. The thickness of polyurea coating is set as 10 mm.

The impact and rear face deflections at mid-span are plotted as functions of coating area ratio in Fig. 19**a** ~ **b**. The impact-side coated

panels exhibit significantly different coating area sensitivity of permanent deflection relative to rear-side coated panels. For the former, both the impact and rear face deflections decrease with increasing coating area ratio. Unfortunately, for the latter, the permanent deformations are insensitive to the dimension of polyurea coating when the coating area ratio exceeds 0.4. Consequently, proper selection of coating position and area ratio should be exercised to achieve optimal shock resistance. Fig. 19**c** ~ **d** display the absorbed energy and energy absorption ratio of each sandwich component. Retrofitting with polyurea markedly reduces the total plastic energy dissipation. With the increase of coating area ratio, the contribution of impact-side polyurea reinforcing to shock energy absorption increases, whereas that of rear-side polyurea firstly increases and then varies slightly.

4.3.4. Effect of coating position
The above discussions conclude that the protective effect of polyurea coating depends on its position on the face sheet of a sandwich panel. Both experiments and computations demonstrate that applying polyurea coating to the impact side, rather than the rear side, is more effective in mitigating the deflection of either the impact or rear face sheet. However, is there any possibility of achieving better shock resistance by applying polyurea coating on both face sheets? To explore this issue, similar to our previous study [50], a coating thickness ratio is defined to quantify the distribution of impact-side and rear-side polyurea coating, with the total thickness of coating fixed so as to maintain the same weight of sandwich panel. Five different coating thickness ratios, 2/8, 4/6, 5/5, 6/4, and 8/2, are selected in the current work. The total coating thickness is 10 mm. For consistency, the foam projectiles have a fixed density of 380 kg m^{-3} and a fixed impact velocity of 300 m s^{-1} (momentum per unit area 9.7 kPa s).

Fig. 20**a** ~ **b** plot the impact and rear face deflections at mid-span as functions of coating thickness ratio. It is seen that smaller panel deformation can be achieved through allocating more polyurea elastomer to the impact face instead of the rear face. In contrast with rear-side coated panels, the permanent impact and rear face deflections of both-side equally coated panels are reduced by 5.2% and 8.2%, respectively. The absorbed energy and energy absorption ratio of each sandwich component are presented in Fig. 20**c** ~ **d**. As with the above analysis, the role of polyurea coating in dissipating shock energy increases by allocating more polyurea elastomer to the impact side. For both-side equally coated panels, the absorbed energy and energy absorption ratio of polyurea elastomer increase by 65.1% and 81.3% relative to rear-side coated panels, respectively.

5. Enhancement mechanisms

As previously mentioned, a dynamically loaded sandwich is brought to rest by plastic bending and longitudinal stretching at the end of core compression. Plastic deformation accumulated in this dynamic stage plays a dominant role in determining the permanent deflection of face sheets. Consequently, figuring out the role of polyurea coating in this stage is essential to interrogate the mechanisms underlying the enhanced shock resistance of polyurea-coated sandwich panels.

Recall the classical theory proposed by Fleck and Deshpande [11]. After the instant that both face sheets have the same velocity, the plastic dynamic behavior of a compressed sandwich panel strongly depends on its yielding locus. For simplicity, in terms of plastic bending moment M_p and plastic membrane force N_p, the yielding locus can be written as:

$$\left| \frac{M}{M_p} \right| + \left| \frac{N}{N_p} \right| = 1 \tag{9}$$

where M and N are the bending moment and membrane force per unit length, respectively. In addition, the sandwich core is assumed to have an average core compressive strain ε_c. As a result, the plastic bending moment M_p can be expressed by:
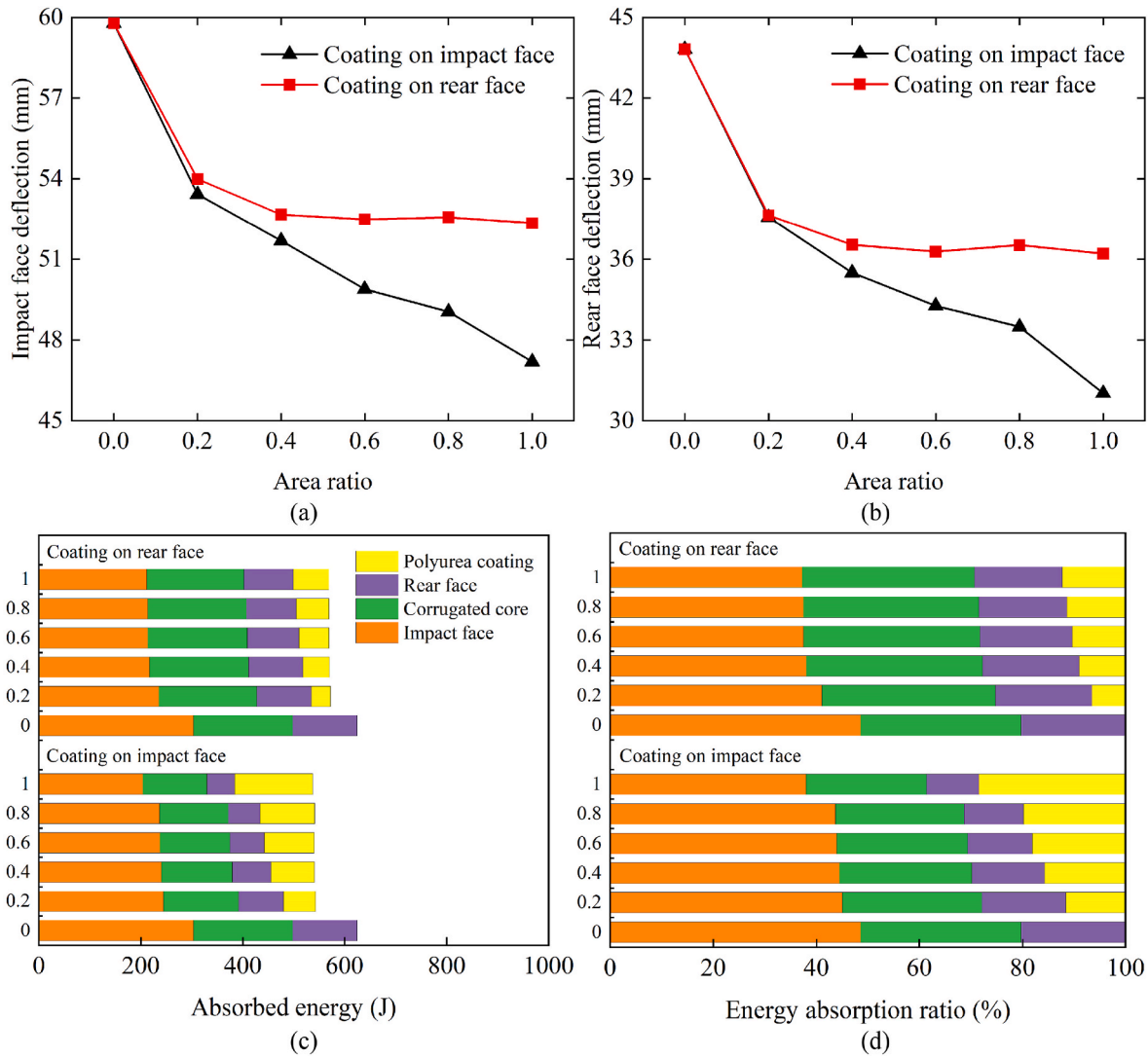
Fig. 19. Shock resistance as a function of coating area: mid-span permanent deflection of (a) impact face and (b) rear face, and (c) absorbed energy and (d) energy absorption ratio of each sandwich component.

$$M_{\mathrm{p}} = \sigma_{\mathrm{fY}} t_{\mathrm{f}} \left[H_{\mathrm{c}}(1 - \varepsilon_{\mathrm{c}}) + t_{\mathrm{f}} \right] + \sigma_{\mathrm{lY}} \frac{H_{\mathrm{c}}^2 (1 - \varepsilon_{\mathrm{c}})}{4} \quad (10)$$

where σ_{fY}, σ_{lY} represent the yield strength of face sheets and the longitudinal tensile strength of sandwich core, and t_{f}, H_{c} denote the thickness of face sheets and the height of sandwich core. Further, upon the assumption that the plastic membrane force is insensitive to core compression [63], the expression of N_{p} can be given by:

$$N_{\mathrm{p}} = \sigma_{\mathrm{lY}} H_{\mathrm{c}} + 2\sigma_{\mathrm{fY}} t_{\mathrm{f}} \quad (11)$$

Based on Eq. (9), it is concluded that the yielding locus of a sandwich panel can be enlarged by increasing its plastic bending moment M_{p} and plastic membrane force N_{p}, thus enhancing its shock resistance. Nevertheless, the dominant roles played by bending and stretching in plastic yielding of an all-metallic sandwich panel can change as its permanent deflection becomes sufficiently large. In general, when the permanent deflection of a sandwich panel is larger than its thickness, membrane stretching dominates the plastic deformation [64]. Conversely, the contribution of plastic bending is more significant to the overall deformation than membrane stretching.

Built upon the above theoretical analysis, how polyurea coating achieves its mitigation effect on impact deformation is qualitatively elucidated. As discussed before, over a wide range of projectile mo-

mentum, polyurea-coated sandwiches display smaller permanent deflections relative to non-coated ones, and the benefit of polyurea coating is sensitive to coating thickness and area. Based on Eqs. (10)–(11), both the plastic bending moment M_{p} and plastic membrane force N_{p} positively correlate with the yielding strength and thickness of face sheets. Whether the deformation is dominated by bending or membrane stretching, improving the stretching resistance of face sheets is beneficial to sandwich panels against shock loading. Accordingly, the existence of perfectly bonded polyurea coating leads to enhanced resistance of face sheets against longitudinal stretching, thus reducing the permanent deflection. Increasing the coating thickness and area further elevates the tensile strength of face sheets and hence the shock resistance of the sandwich. These mechanisms are also helpful for understanding why the strategy of constructing hybrid sandwich cores is less effective for sandwich structures experiencing large impact deformation [25,26]: large plastic deformation is usually dominated by plastic membrane force, whereas the corresponding contribution of the hybrid core is small due to its relatively low tensile strength (seen in Eq. (11)). When plastic deformation is dominated by bending, the compressive strain ε_{c} of the cellular core can be somewhat curtailed by filling certain materials (e.g., foam [33], water [25], and sand [26]) into the core, leading to larger plastic bending moment (seen in Eq. (10)). Nevertheless, core filling will also lessen its capacity for energy absorption. In a
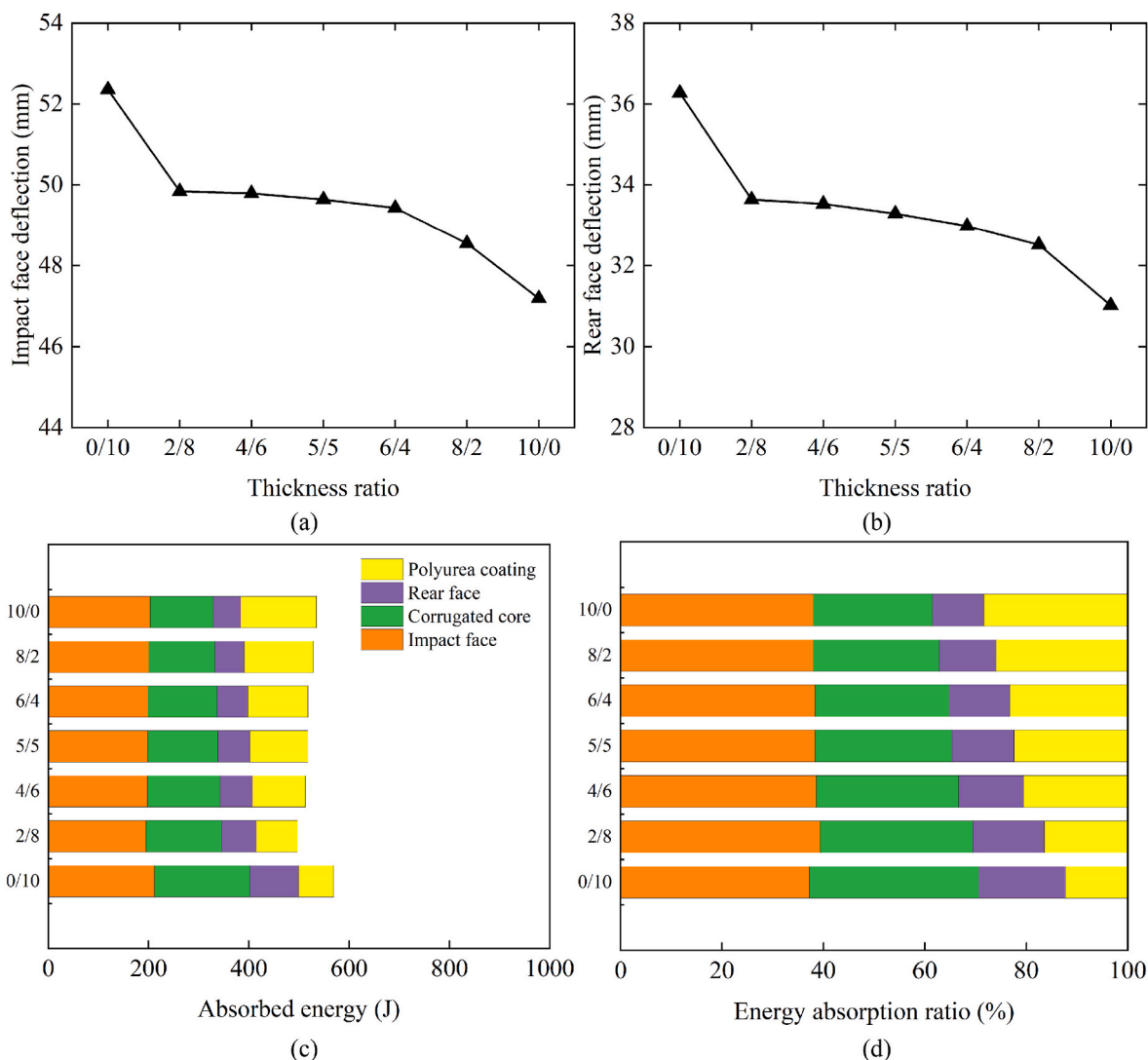
Fig. 20. Shock resistance as a function of coating position: mid-span permanent deflection of (a) impact face and (b) rear face, and (c) absorbed energy and (d) energy absorption ratio of each sandwich component.

word, strengthening the face sheets rather than the core appears to be particularly effective for sandwich construction against intense shock loading.

Another important finding of the current study is that, under the constraint of fixed total coating thickness, a better shock resistance can be achieved by allocating more polyurea coating on the impact face, rather than the rear face. As illustrated in Fig. 12, whether polyurea reinforcing is placed on the impact or rear side, the momentum transferred to the sandwich is approximately the same, equal to the initial projectile momentum. As a result, the initial shock effect caused by the impedance of foam projectiles, polyurea coating, and metal face sheets can not account for the current cases. For clarification, consider geometrically asymmetric sandwich panels against blast loading. Both theoretically and experimentally, it has been elucidated that an appropriate sequence of asymmetric face sheets (i.e., thick impact face and thin rear face) leads to markedly enhanced blast resistance of sandwich panels [61,65]. Accordingly, the sensitivity of coating position might be attributed to the fact that placing more polyurea on the impact face creates a sandwich with asymmetric face sheets, thus improving its shock resistance. However, it might not be cost-efficient to retrofit a sandwich construction with polyurea coating that is too thick. Therefore, how to enhance the dynamic stretching resistance of polyurea elastomer without sacrificing its ductility will be a topic of interest for

practical applications.

6. Concluding remarks

The primary motivation of this investigation is to evaluate the effectiveness of polyurea coating on resisting structural deformation of all-metallic corrugated core sandwich panels subjected to shock loading. A combined experimental and numerical tool has been adopted to quantify the benefits of polyurea reinforcing and interrogate the mechanisms by which polyurea coating achieves its mitigation effect. As follows, four primary conclusions are established:

(i) The strategy of using polyurea coating to enhance the shock resistance of all-metallic sandwich construction is proposed for the first time. Experimental results reveal that retrofitting a sandwich panel with polyurea coating helps curtail permanent deflection in its central region and shear failure around its clamped edges.

(ii) High-fidelity finite element models established (with both rate-dependent compressive and tensile behaviors of polyurea elastomer accounted for) provide accurate predictions on dynamic responses of non-coated and coated sandwich panels under foam projectile impact.

(iii) For shock loadings varying over a wide range, the mitigation effect of polyurea coating on structural deformation remains stable. The benefit of polyurea coating is sensitive to coating thickness, area, and position, and the use of thicker, larger, and impact-side polyurea coating is preferred.

(iv) The enhanced shock resistance of polyurea-coated sandwich panel is attributed to the mechanism that the presence of polyurea coating improves both the plastic bending moment and plastic membrane force of the sandwich, thus enlarging its yielding locus.

Author statement

Xin Wang: Conceptualization, Methodology, Software, Writing - Original Draft, Writing - Review & Editing., **Chao He:** Investigation, Data curation., **Zengshen Yue:** Investigation, Validation., **Xue Li:** Investigation., **Runpei Yu:** Methodology., **Haibo Ji:** Software., **Zhenyu Zhao:** Software., **Qiancheng Zhang:** Supervision, Writing - Review & Editing., **Tian Jian Lu:** Supervision, Funding acquisition, Writing - Review & Editing.

Declaration of competing interest

The authors declare that they have no known competing financial interests or personal relationships that could have appeared to influence the work reported in this paper.

Appendix A. Constitutive relationships used in FE simulations

A.1. Stainless steel

The 304 stainless steel face sheets are modeled by isotropic J2-flow theory rate-dependent solids with density $\rho_s = 7800 \ \mathrm{kg \ m^{-3}}$, Young's modulus $E_s = 200$ GPa, Poisson's ratio $\mu_s = 0.3$, yield strength $\sigma_y = 180$ MPa, and tangent modulus $E_t = 1.8$ GPa. The effect of strain rate on equivalent stress σ_{eq} is attained by multiplying the quasi-static response σ_0 by a dynamic enhancement factor R, as:

$$\sigma_{eq}\left(\varepsilon_{pl}, \dot{\varepsilon}_{pl}\right) = R\left(\dot{\varepsilon}_{pl}\right)\sigma_0\left(\varepsilon_{pl}\right) \tag{A.1}$$

where ε_{pl} and $\dot{\varepsilon}_{pl}$ is equivalent plastic strain and strain rate, respectively. Recall that the quasi-static true stress versus strain relation of 304 stainless steel is presented in Fig. 3a. Similar to a previous study [66], the dynamic strength enhancement factor used in the current simulation is plotted as a function of equivalent plastic strain rate in Fig. A1.
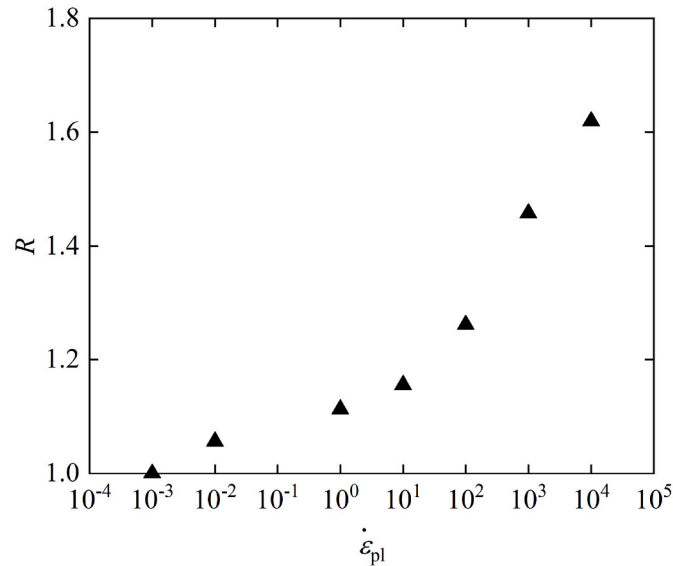
Fig. A1. Dynamic strength enhancement ratio R plotted as a function of strain rate for 304 stainless steel [66].

A.2. Aluminum foam

Aluminum foam projectiles are modeled by isotropic compressible continuums based on the rate-dependent Deshpande-Fleck (D-F) model [67]. An isotropic yield surface of the metal foam can be expressed by:

$$\sigma_{eq} - Y = 0 \tag{A.2}$$

The D-F model assumes that the equivalent stress σ_{eq} is associated with the von Mises stress σ_{vm} and the mean stress σ_m, as:

$$\sigma_{\text{eq}}^2 = \frac{1}{1 + (\alpha/3)^2} \left[\sigma_{\text{vm}}^2 + \alpha^2 \sigma_{\text{m}}^2 \right] \tag{A.3}$$

where α denotes the ratio of deviatoric strength to hydrostatic strength. To consider the strain rate sensitivity of metal foam, a simple over-stress equation is accepted to express the yield stress Y, as:

$$Y = \sigma_0 + \eta \dot{\varepsilon}_{\text{p}} \tag{A.4}$$

where η is the viscosity of metal foam, expressed by Ref. [57]:

$$\eta = \frac{\rho_{\text{f}} w \Delta v}{\varepsilon_{\text{d}}} \tag{A.5}$$

Here, ρ_{f} is the foam density and w is set as one-tenth of projectile length l_0. The densification strain ε_{d} is obtained from Fig. 3b, while the velocity jump across the shock Δv can be approximated by the initial impact velocity v_0. The plastic strain rate $\dot{\varepsilon}_{\text{p}}$ is work conjugate to the equivalent stress σ_{eq}, and the quasi-static response σ_0 is directly obtained from the experimental data plotted in Fig. A2. Additionally, the D-F model defines the plastic Poisson's ratio μ_{fp}, as:

$$\mu_{\text{fp}} = \frac{1/2 - (\alpha/3)^2}{1 + (\alpha/3)^2} \tag{A.6}$$

In the current work, the foam projectile is assumed to have mass density $\rho_{\text{f}} = 380$ kg m^{-3}, Young's modulus $E_{\text{f}} = 1$ GPa, elastic Poisson's ratio $\mu_{\text{fe}} = 0.3$, plastic Poisson's ratio $\mu_{\text{fp}} = 0$, and densification strain $\varepsilon_{\text{d}} = 0.55$. Note that the projectile stiffness is not associated with the pressure pulse produced by the foam projectile [57].
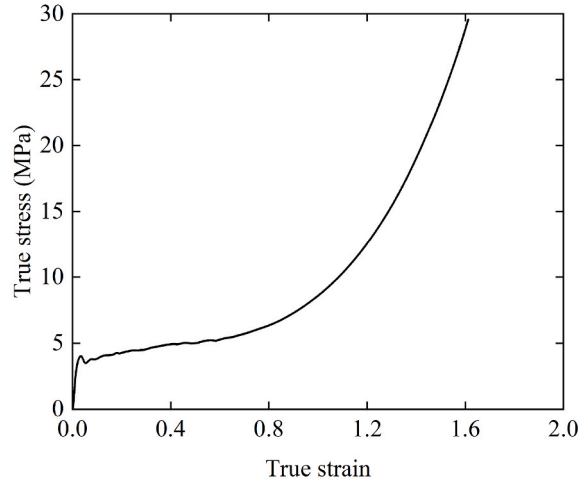

Fig. A2. Quasi-static true stress versus true (logarithmic) strain relation of aluminum foam.

A.3. Polyurea elastomer

As with our previous theoretical effort [54], Qtech-420 polyurea elastomer is modeled using a compressible visco-hyperelastic model implemented via a user-defined material (VUMAT) subroutine. The Cauchy stress $\boldsymbol{\sigma}^{\text{vh}}$ can be divided into two parts, i.e., a five-parameter hyperelastic component $\boldsymbol{\sigma}^{\text{he}}$ and a three-parameter viscoelastic component $\boldsymbol{\sigma}^{\text{ve}}$, as:

$$\boldsymbol{\sigma}^{\text{vh}} = \boldsymbol{\sigma}^{\text{he}} + \boldsymbol{\sigma}^{\text{ve}} \tag{A.7}$$

The rate-insensitive hyperelastic stress tensor $\boldsymbol{\sigma}^{\text{he}}$ can be derived by:

$$\boldsymbol{\sigma}^{\text{he}} = -2 \left(\left(A_2 + A_3 \left(J^{-\frac{2}{3}} I_1 - 3 \right) \right) J^{-\frac{7}{3}} \right) \mathbf{B}^2$$
$$+ 2 \left(\left(A_1 + A_4 e^{-A_5 \left(J^{-\frac{2}{3}} I_1 - 3 \right)} \right) J^{-\frac{5}{3}} + \left(A_2 + A_3 \left(J^{-\frac{2}{3}} I_1 - 3 \right) \right) J^{-\frac{7}{3}} I_1 + A_3 \left(J^{-\frac{4}{3}} I_2 - 3 \right) J^{-\frac{5}{3}} \right) \mathbf{B} \tag{A.8}$$
$$+ \left(2D(J - 1) - \frac{2}{3} \left(A_1 + A_4 e^{-A_5 \left(J^{-\frac{2}{3}} I_1 - 3 \right)} \right) J^{-\frac{5}{3}} I_1 - \frac{4}{3} \left(A_2 + A_3 \left(J^{-\frac{2}{3}} I_1 - 3 \right) \right) J^{-\frac{7}{3}} I_2 - \frac{2}{3} A_3 \left(J^{-\frac{4}{3}} I_2 - 3 \right) J^{-\frac{5}{3}} \right) \mathbf{I}$$

where **B** is the left Cauchy-Green deformation tensor, **I** is the unit tensor, I_1 and I_2 are the first two invariants of the right Cauchy-Green deformation tensor **C**, and J is the Jacobian determinant of deformation gradient **F**. Further, the rate-sensitive viscoelastic stress tensor $\boldsymbol{\sigma}^{\text{ve}}$ can be written by:

$$\boldsymbol{\sigma}^{\text{ve}} = \frac{2(1 + \mu)}{3(1 - 2\mu)} \left(G_\infty \varepsilon_{\text{v}} + G_1 \int_0^t e^{-\frac{t - \tau}{\theta_1}} \dot{\varepsilon}_{\text{v}} d\tau \right) \mathbf{I} + 2 \left(G_\infty \mathbf{s}^{\text{ve}} + G_1 \int_0^t e^{-\frac{t - \tau}{\theta_1}} \dot{\mathbf{s}}^{\text{ve}} d\tau \right) \tag{A.9}$$

where ε_v and s^{ve} are the volumetric and deviatoric strain, while $\dot{\varepsilon}_v$ and $\dot{s}^{ve}$ are the volumetric and deviatoric strain rate. The three-dimensional form of Cauchy stress tensor in Eq. (A.7) can be rewritten into a one-dimensional equation for uniaxial deformation (Poisson's ratio $\mu = 0.485$ for numerical reasons [68]), as:

$$
\sigma_{11} = 2\left(\frac{A_2}{\lambda^{2.01}} + \frac{A_1 + A_4 e^{-A_5\left(-3+\frac{2}{\lambda^{0.99}}+\lambda^{1.98}\right)}}{\lambda^{1.02}} \right)\left(-1+\lambda^{2.97}\right) + \frac{6A_3\left(-\lambda^{3.03}+\lambda^{4.02}+\lambda^{5.01}-\lambda^{6.99}-\lambda^{7.98}+\lambda^{8.97}\right)}{\lambda^{6.03}}
$$
$$
+ 2G_\infty\left(\lambda - \lambda^{-0.485}\right) + 2G_1\int_0^t\left(1+0.485\lambda^{-1.485}\right)\dot{\lambda}e^{-\frac{t-\tau}{\theta_1}}d\tau
$$

(A.10)

where λ is the stretch at loading direction, and $A_1, A_2, A_3, A_4, A_5, G_\infty, G_1$ and θ_1 are model constants evaluated from quasi-static and dynamic compressive and tensile results shown in Fig. 4. Figure A3 compares the experimental and fitted results at selected strain rates. Corresponding optimal model parameters are listed in Table A1.
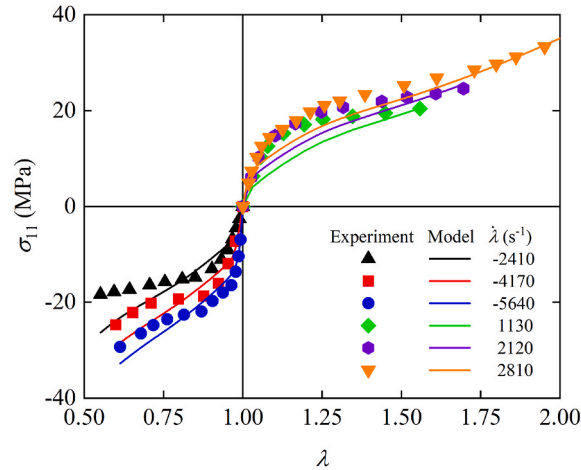

Fig. A3. Comparison between experimental and predicted results of mechanical response of polyurea elastomer at selected strain rates.

Table A1
Visco-hyperelastic model parameters of Qtech-420 polyurea elastomer.

A_1 (MPa)	A_2 (MPa)	A_3 (MPa)	A_4 (MPa)	A_5	G_∞ (MPa)	G_1 (MPa)	θ_1 (µs)
1.107	0.231	0.0344	3.772	3.221	8.308	446.388	1.658

Appendix B. Influence of impact position on structural deformation

The influence of impact position on the dynamic response of non-coated corrugated core sandwich panels is numerically analyzed here. As shown in Fig. B1, the sandwich panels are impacted at either a brazing joint of a corrugated core or mid-way between two joints. For clarity, these two loading conditions are denoted as joint impact and span impact, respectively. Upon the verified FE model, five different impact velocities (100, 150, 200, 250, and 300 m s^{-1}) of foam projectiles with an identical density of 380 kg m^{-3} are dynamically imparted on the sandwich panels. The mid-span permanent deflections of sandwich panels are presented in Fig. B2. It is clearly testified that both impact and rear face deflections are not sensitive to the impact position, and the difference can be ignored. Therefore, only the joint impact loading is adopted in this work.
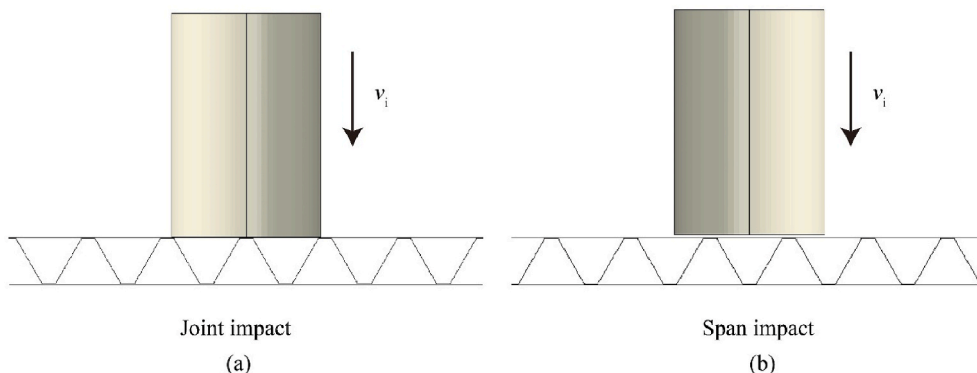

Joint impact
(a)

Span impact
(b)

Fig. B1. FE models of non-coated panels under two loading conditions: (a) joint impact and (b) span impact.
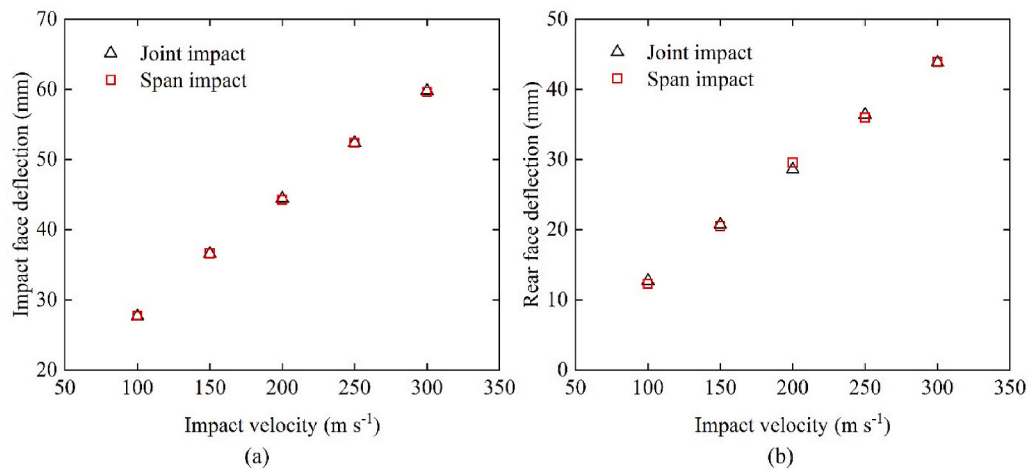
Fig. B2. Predicted permanent deformation of (a) impact face and (b) rear face.

References

[1] Dharmasena KP, Wadley HNG, Xue Z, Hutchinson JW. Mechanical response of metallic honeycomb sandwich panel structures to high-intensity dynamic loading. Int J Impact Eng 2008;35:1063–74. https://doi.org/10.1016/j.ijimpeng.2007.06.008.

[2] Dharmasena KP, Wadley HNG, Williams K, Xue Z, Hutchinson JW. Response of metallic pyramidal lattice core sandwich panels to high intensity impulsive loading in air. Int J Impact Eng 2011;38:275–89. https://doi.org/10.1016/j.ijimpeng.2010.10.002.

[3] Wadley HNG, Borvik T, Olovsson L, Wetzel JJ, Dharmasena KP, Hopperstad OS, et al. Deformation and fracture of impulsively loaded sandwich panels. J Mech Phys Solid 2013;61:674–99. https://doi.org/10.1016/j.jmps.2012.07.007.

[4] Wang H, Long S, Yao X, Lu G, Zhang X, Han Q. Analytical study on the low-velocity impact penetration of the fully-clamped foam-core composite sandwich panels. Compos B Eng 2021;224:109214. https://doi.org/10.1016/j.compositesb.2021.109214.

[5] Sun G, Huo X, Wang H, Hazell PJ, Li Q. On the structural parameters of honeycomb-core sandwich panels against low-velocity impact. Compos B Eng 2021;216:108881. https://doi.org/10.1016/j.compositesb.2021.108881.

[6] Sun M, Wowk D, Mechefske C, Alexander E, Kim IY. Surface and honeycomb core damage in adhesively bonded aluminum sandwich panels subjected to low-velocity impact. Compos B Eng 2022;230:109506. https://doi.org/10.1016/j.compositesb.2021.109506.

[7] Odessa I, Frostig Y, Rabinovitch O. Dynamic interfacial debonding in sandwich panels. Compos B Eng 2020;185:107733. https://doi.org/10.1016/j.compositesb.2019.107733.

[8] Peng C, Tran P. Bioinspired functionally graded gyroid sandwich panel subjected to impulsive loadings. Compos B Eng 2020;188:107773. https://doi.org/10.1016/j.compositesb.2020.107773.

[9] Zhang C, Tan KT. Low-velocity impact response and compression after impact behavior of tubular composite sandwich structures. Compos B Eng 2020;193:108026. https://doi.org/10.1016/j.compositesb.2020.108026.

[10] Hutchinson JW, Xue Z. Metal sandwich plates optimized for pressure impulses. Int J Mech Sci 2005;47:545–69. https://doi.org/10.1016/j.ijmecsci.2004.10.012.

[11] Fleck NA, Deshpande VS. The resistance of clamped sandwich beams to shock loading. J Appl Mech 2004;71:386. https://doi.org/10.1115/1.1629109.

[12] Rathbun HJ, Radford DD, Xue Z, He MY, Yang J, Deshpande V, et al. Performance of metallic honeycomb-core sandwich beams under shock loading. Int J Solid Struct 2006;43:1746–63. https://doi.org/10.1016/j.ijsolstr.2005.06.079.

[13] Betts D, Sadeghian P, Fam A. Experiments and nonlinear analysis of the impact behaviour of sandwich panels constructed with flax fibre-reinforced polymer faces and foam cores. J Sandw Struct Mater 2021;23:3139–63. https://doi.org/10.1177/1099636220925073.

[14] Sharaf T, Fam A. Experimental investigation of large-scale cladding sandwich panels under out-of-plane transverse loading for building applications. J Compos Construct 2011;15:422–30. https://doi.org/10.1061/(asce)cc.1943-5614.0000176.

[15] Sun ZP, Guo YB, Shim VPW. Characterisation and modeling of additively-manufactured polymeric hybrid lattice structures for energy absorption. Int J Mech Sci 2021;191:106101. https://doi.org/10.1016/j.ijmecsci.2020.106101.

[16] Ha NS, Lu G. A review of recent research on bio-inspired structures and materials for energy absorption applications. Compos B Eng 2020;181:107496. https://doi.org/10.1016/j.compositesb.2019.107496.

[17] Qi C, Jiang F, Remennikov A, Pei LZ, Liu J, Wang JS, et al. Quasi-static crushing behavior of novel re-entrant circular auxetic honeycombs. Compos B Eng 2020;197:108117. https://doi.org/10.1016/j.compositesb.2020.108117.

[18] Zhang J, Lu G, You Z. Large deformation and energy absorption of additively manufactured auxetic materials and structures: a review. Compos B Eng 2020;201:108340. https://doi.org/10.1016/j.compositesb.2020.108340.

[19] Quan C, Han B, Hou Z, Zhang Q, Tian X, Lu TJ. 3D printed continuous fiber reinforced composite auxetic honeycomb structures. Compos B Eng 2020;187:107858. https://doi.org/10.1016/j.compositesb.2020.107858.

[20] Zhang P, Cheng Y, Liu J, Wang C, Hou H, Li Y. Experimental and numerical investigations on laser-welded corrugated-core sandwich panels subjected to air blast loading. Mar Struct 2015;40:225–46. https://doi.org/10.1016/j.marstruc.2014.11.007.

[21] McShane GJ, Deshpande VS, Fleck NA. The underwater blast resistance of metallic sandwich beams with prismatic lattice cores. J Appl Mech 2007;74:352. https://doi.org/10.1115/1.2198549.

[22] Wadley HNG, Borvik T, Olovsson L, Wetzel JJ, Dharmasena KP, Hopperstad OS, et al. Deformation and fracture of impulsively loaded sandwich panels. J Mech Phys Solid 2013;61:674–99. https://doi.org/10.1016/j.jmps.2012.07.007.

[23] Rubino V, Deshpande VS, Fleck NA. The dynamic response of end-clamped sandwich beams with a Y-frame or corrugated core. Int J Impact Eng 2008;35:829–44. https://doi.org/10.1016/j.ijimpeng.2007.10.006.

[24] Rubino V, Deshpande VS, Fleck NA. The dynamic response of clamped rectangular Y-frame and corrugated core sandwich plates. Eur J Mech Solid 2009;28:14–24. https://doi.org/10.1016/j.euromechsol.2008.06.001.

[25] Wang X, Yu RP, Zhang QC, Li L, Li X, Zhao ZY, et al. Dynamic response of clamped sandwich beams with fluid-filled corrugated cores. Int J Impact Eng 2020;139:103533. https://doi.org/10.1016/j.ijimpeng.2020.103533.

[26] Yu R, Wang X, Zhang Q, Li L, He S, Han B, et al. Effects of sand filling on the dynamic response of corrugated core sandwich beams under foam projectile impact. Compos Part B 2020;197:108135. https://doi.org/10.1016/j.compositesb.2020.108135.

[27] Tilbrook MT, Radford DD, Deshpande VS, Fleck NA. Dynamic crushing of sandwich panels with prismatic lattice cores. Int J Solid Struct 2007;44:6101–23. https://doi.org/10.1016/j.ijsolstr.2007.02.015.

[28] McShane GJ, Pingle SM, Deshpande VS, Fleck NA. Dynamic buckling of an inclined strut. Int J Solid Struct 2012;49:2830–8. https://doi.org/10.1016/j.ijsolstr.2012.03.045.

[29] Li X, Wang Z, Zhu F, Wu G, Zhao L. Response of aluminium corrugated sandwich panels under air blast loadings: experiment and numerical simulation. Int J Impact Eng 2014;65:79–88. https://doi.org/10.1016/j.ijimpeng.2013.11.002.

[30] Xue Z, Hutchinson JW. A comparative study of impulse-resistant metal sandwich plates. Int J Impact Eng 2004;30:1283–305. https://doi.org/10.1016/j.ijimpeng.2003.08.007.

[31] Han B, Zhang ZJ, Zhang QC, Zhang Q, Lu TJ, Lu BH. Recent advances in hybrid lattice-cored sandwiches for enhanced multifunctional performance. Extrem Mech Lett 2017;10:58–69. https://doi.org/10.1016/j.eml.2016.11.009.

[32] Cheng Y, Liu M, Zhang P, Xiao W, Zhang C, Liu J, et al. The effects of foam filling on the dynamic response of metallic corrugated core sandwich panel under air blast loading – experimental investigations. Int J Mech Sci 2018;145:378–88. https://doi.org/10.1016/j.ijmecsci.2018.07.030.

[33] Zhang P, Cheng Y, Liu J, Li Y, Zhang C, Hou H, et al. Experimental study on the dynamic response of foam-filled corrugated core sandwich panels subjected to air blast loading. Compos B Eng 2016;105:67–81. https://doi.org/10.1016/j.compositesb.2016.08.038.

[34] Børvik T, Burbach A, Langberg H, Langseth M. On the ballistic and blast load response of a 20ft ISO container protected with aluminium panels filled with a

local mass - phase II: Validation of protective system. Eng Struct 2008;30:1621–31. https://doi.org/10.1016/j.engstruct.2007.10.011.

[35] Ni CY, Li YC, Xin FX, Jin F, Lu TJ. Ballistic resistance of hybrid-cored sandwich plates: numerical and experimental assessment. Compos Part A Appl Sci Manuf 2013;46:69–79. https://doi.org/10.1016/j.compositesa.2012.07.019.

[36] Ni CY, Hou R, Xia HY, Zhang QC, Wang WB, Cheng ZH, et al. Perforation resistance of corrugated metallic sandwich plates filled with reactive powder concrete: experiment and simulation. Compos Struct 2015;127:426–35. https://doi.org/10.1016/j.compstruct.2015.02.059.

[37] Iqbal N, Tripathi M, Parthasarathy S, Kumar D, Roy PK. Polyurea coatings for enhanced blast-mitigation: a review. RSC Adv 2016;6:109706–17. https://doi.org/10.1039/c6ra23866a.

[38] Porter J, Dinan R, Hammons M, Knox K. Polymer coatings increase blast resistance of existing and temporary structures. Amptiac Q 2002;6:47–52.

[39] Tekalur SA, Shukla A, Shivakumar K. Blast resistance of polyurea based layered composite materials. Compos Struct 2008;84:271–81. https://doi.org/10.1016/j.compstruct.2007.08.008.

[40] Iqbal N, Sharma PK, Kumar D, Roy PK. Protective polyurea coatings for enhanced blast survivability of concrete. Construct Build Mater 2018;175:682–90. https://doi.org/10.1016/j.conbuildmat.2018.04.204.

[41] Xue Z, Hutchinson JW. Neck retardation and enhanced energy absorption in metal-elastomer bilayers. Mech Mater 2007;39:473–87. https://doi.org/10.1016/j.mechmat.2006.08.002.

[42] Xue Z, Hutchinson JW. Neck development in metal/elastomer bilayers under dynamic stretchings. Int J Solid Struct 2008;45:3769–78. https://doi.org/10.1016/j.ijsolstr.2007.10.006.

[43] Amini MR, Isaacs JB, Nemat-Nasser S. Experimental investigation of response of monolithic and bilayer plates to impulsive loads. Int J Impact Eng 2010;37:82–9. https://doi.org/10.1016/j.ijimpeng.2009.04.002.

[44] Amini MR, Simon J, Nemat-Nasser S. Investigation of effect of polyurea on response of steel plates to impulsive loads in direct pressure-pulse experiments. Mech Mater 2010;42:615–27. https://doi.org/10.1016/j.mechmat.2009.09.009.

[45] Ackland K, Anderson C, Ngo TD. Deformation of polyurea-coated steel plates under localised blast loading. Int J Impact Eng 2013;51:13–22. https://doi.org/10.1016/j.ijimpeng.2012.08.005.

[46] Grujicic M, Snipes JS, Ramaswami S, Yavari R, Ramasubramanian MK. Meso-scale computational investigation of shock-wave attenuation by trailing release wave in different grades of polyurea. J Mater Eng Perform 2014;23:49–64. https://doi.org/10.1007/s11665-013-0760-3.

[47] Grujicic M, D'Entremont BP, Pandurangan B, Runt J, Tarter J, Dillon G. Concept-level analysis and design of polyurea for enhanced blast-mitigation performance. J Mater Eng Perform 2012;21:2024–37. https://doi.org/10.1007/s11665-011-0117-8.

[48] Grujicic M, Pandurangan B, Bell WC, Cheeseman BA, Yen CF, Randow CL. Molecular-level simulations of shock generation and propagation in polyurea. Mater Sci Eng, A 2011;528:3799–808. https://doi.org/10.1016/j.msea.2011.01.081.

[49] Grujicic M, Yavari R, Snipes JS, Ramaswami S, Runt J, Tarter J, et al. Molecular-level computational investigation of shock-wave mitigation capability of polyurea. J Mater Sci 2012;47:8197–215. https://doi.org/10.1007/s10853-012-6716-4.

[50] Wang X, Li X, Yu RP, Ren JW, Zhang QC, Zhao ZY, et al. Enhanced vibration and damping characteristics of corrugated sandwich panels with polyurea-metal laminate face sheets. Compos Stuctures 2020;251:112591. https://doi.org/10.1016/j.compstruct.2020.112591.

[51] Wang X, Li X, Yue Z, Yu R, Zhang Q, Du S, et al. Optimal design of metallic corrugated sandwich panels with polyurea-metal laminate face sheets for simultaneous vibration attenuation and structural stiffness. Compos Struct 2020; 256:112994. https://doi.org/10.1016/j.compstruct.2020.112994.

[52] Andrews EW, Gioux G, Onck P, Gibson LJ. Size effects in ductile cellular solids. Part II: experimental results. Int J Mech Sci 2001;43:701–13. https://doi.org/10.1016/S0020-7403(00)00043-6.

[53] Miltz J, Ramon OR. Energy absorption characteristics of polymeric foams used as cushioning materials. Polym Eng Sci 1990;30:129–33.

[54] Wang X, Ji H, Li X, Sun S, Zhang Q, Shim VPW, et al. Static and dynamic compressive and tensile response of highly stretchable polyurea. Submitted for publication; 2021.

[55] Rusty GT Iii G, Blumenthal WR. Split-hopkinson pressure bar testing of soft materials. Mech Test Eval 2018;8:488–96. https://doi.org/10.31399/asm.hb.v08.a0003298.

[56] McShane GJ, Stewart C, Aronson MT, Wadley HNG, Fleck NA, Deshpande VS. Dynamic rupture of polymer-metal bilayer plates. Int J Solid Struct 2008;45:4407–26. https://doi.org/10.1016/j.ijsolstr.2008.03.017.

[57] Radford DD, Deshpande VS, Fleck NA. The use of metal foam projectiles to simulate shock loading on a structure. Int J Impact Eng 2005;31:1152–71. https://doi.org/10.1016/j.ijimpeng.2004.07.012.

[58] Jacob N, Nurick GN, Langdon GS. The effect of stand-off distance on the failure of fully clamped circular mild steel plates subjected to blast loads. Eng Struct 2007; 29:2723–36. https://doi.org/10.1016/j.engstruct.2007.01.021.

[59] Zhang P, Liu J, Cheng Y, Hou H, Wang C, Li Y. Dynamic response of metallic trapezoidal corrugated-core sandwich panels subjected to air blast loading - an experimental study. Mater Des 2015;65:221–30. https://doi.org/10.1016/j.matdes.2014.08.071.

[60] Chen C, Wang X, Hou H, Cheng Y, Zhang P, Liu J. Effect of strength matching on failure characteristics of polyurea coated thin metal plates under localized air blast loading: experiment and numerical analysis. Thin-Walled Struct 2020;154:106819. https://doi.org/10.1016/j.tws.2020.106819.

[61] Wang T, Ma M, Yu W, Dong S, Gao Y. Mechanical response of square honeycomb sandwich plate with asymmetric face sheet subjected to blast loading. Procedia Eng 2011;23:457–63. https://doi.org/10.1016/j.proeng.2011.11.2530.

[62] Longère P, Geffroy-Grèze AG, Leblé B, Dragon A. Ship structure steel plate failure under near-field air-blast loading: numerical simulations vs experiment. Int J Impact Eng 2013;62:88–98. https://doi.org/10.1016/j.ijimpeng.2013.06.009.

[63] Qin Q, Yuan C, Zhang J, Wang TJ. Large deflection response of rectangular metal sandwich plates subjected to blast loading. Eur J Mech Solid 2014;47:14–22. https://doi.org/10.1016/j.euromechsol.2014.02.016.

[64] Qin Q, Yuan C, Zhang J, Wang TJ. A simplified analytical model for metal sandwich beam with soft core under impulsive loading over a central patch. Int J Impact Eng 2014;74:67–82. https://doi.org/10.1016/j.ijimpeng.2014.06.008.

[65] Wang T, Qin Q, Wang M, Yu W, Wang J, Zhang J, et al. Blast response of geometrically asymmetric metal honeycomb sandwich plate: experimental and theoretical investigations. Int J Impact Eng 2017;105:24–38. https://doi.org/10.1016/j.ijimpeng.2016.10.009.

[66] Radford DD, McShane GJ, Deshpande VS, Fleck NA. The response of clamped sandwich plates with metallic foam cores to simulated blast loading. Int J Solid Struct 2006;43:2243–59. https://doi.org/10.1016/j.ijsolstr.2005.07.006.

[67] Deshpande VS, Fleck NA. Isotropic constitutive models for metallic foams. J Mech Phys Solid 2000;48:1253–83. https://doi.org/10.1038/oby.2006.163.

[68] Fallon C, McShane GJ. Fluid-structure interactions for the air blast loading of elastomer-coated concrete. Int J Solid Struct 2019;168:138–52. https://doi.org/10.1016/j.ijsolstr.2019.03.017.